



# HHS Public Access

Author manuscript

*Nat Commun.* Author manuscript; available in PMC 2014 August 18.

Published in final edited form as:

*Nat Commun.* 2014 ; 5: 3263. doi:10.1038/ncomms4263.

## miR-191 and miR-135 are required for long-lasting spine remodeling associated with synaptic long term depression

Zhonghua Hu<sup>1</sup>, Danni Yu<sup>3</sup>, Qin-hua Gu<sup>1</sup>, Yanqin Yang<sup>2</sup>, Kang Tu<sup>2</sup>, Jun Zhu<sup>2</sup>, and Zheng Li<sup>1,†</sup>

<sup>1</sup>Unit on Synapse Development and Plasticity, National Institute of Mental Health, National Institutes of Health, USA

<sup>2</sup>Genetics and Developmental Biology Center, National Heart Lung and Blood Institute, National Institutes of Health, USA

<sup>3</sup>Department of Statistics, Purdue University, USA

### Abstract

Activity-dependent modification of dendritic spines, subcellular compartments accommodating postsynaptic specializations in the brain, is an important cellular mechanism for brain development, cognition and synaptic pathology of brain disorders. NMDA receptor-dependent long-term depression (NMDAR-LTD), a prototypic form of synaptic plasticity, is accompanied by prolonged remodeling of spines. The mechanisms underlying long-lasting spine remodeling in NMDAR-LTD, however, are largely unclear. Here we show that LTD induction causes global changes in miRNA transcriptomes affecting many cellular activities. Specifically, we show that expression changes of miR-191 and miR-135 are required for maintenance but not induction of spine restructuring. Moreover, we find that actin depolymerization and AMPA receptor exocytosis are regulated for extended periods of time by miRNAs to support long-lasting spine plasticity. These findings reveal a novel miRNA mediated-mechanism and a new role of AMPA receptor exocytosis in long-lasting spine plasticity, and identify a number of candidate miRNAs involved in LTD.

---

Dendritic spines are tiny protrusions from dendritic shafts where the majority of excitatory synapses in the central nervous system are located <sup>1</sup>. The size and geometry of dendritic spines are coupled to synaptic strength <sup>2,3</sup>, and are modulated by synaptic activity to

---

Users may view, print, copy, download and text and data- mine the content in such documents, for the purposes of academic research, subject always to the full Conditions of use: [http://www.nature.com/authors/editorial\\_policies/license.html#terms](http://www.nature.com/authors/editorial_policies/license.html#terms)

† Correspondence to: **Zheng Li**, Unit on Synapse Development and Plasticity, National Institute of Mental Health, National Institutes of Health, Bethesda, MD 20892, USA. [lizheng2@mail.nih.gov](mailto:lizheng2@mail.nih.gov); 301.594.2269 (tel); 301.480.2561 (fax).

#### Author contributions

Z. H., J. Z., and Z. L. designed the experiments. Z. H. performed the experiments and analyzed the data. D. Y., Y. Y., and K. T., performed the deep sequencing data analysis and miRNA-gene-GO enrichment analysis. Q. G. performed and analyzed the electrophysiological experiments. Z. H. and Z. L. wrote the manuscript.

#### Competing financial interests

The authors declare no competing financial interests.

#### Accession Codes

The miRNA sequencing data were deposited in the NIH Sequence Read Archive (SRA) database under accession code SRP034860.

accompany the functional change of synapses during synapse development and synaptic plasticity<sup>4</sup>. Activity-induced changes in spines occur in both directions. For instance, long-term depression (LTD) of synaptic transmission is usually associated with spine shrinkage and loss, while long-term potentiation (LTP) of synaptic transmission is characterized by spine enlargement and formation<sup>5, 6</sup>. The changes in dendritic spines during synaptic plasticity can be maintained for prolonged periods of time<sup>5</sup>. Long-lasting modification of dendritic spines is an important cellular mechanism for information storage in the brain<sup>7, 8</sup>.

N-methyl-D-aspartate (NMDA) receptor-dependent LTD (NMDAR-LTD) is a form of synaptic plasticity important for learning and memory. LTD impairment in mice caused by knockout of NMDA receptor subunits or inhibition of NMDA receptor signaling pathways is associated with cognitive deficits, such as dysfunctions in spatial learning, working memory and behavioral flexibility<sup>9–11</sup>. Induction of NMDAR-LTD is accompanied by spine shrinkage and loss. The mechanisms underlying the structural and functional plasticity in LTD overlap partially. For instance, they both require NMDA receptors, calcineurine and actin depolymerization, but AMPA receptor endocytosis and protein phosphatase 1 are only involved in synaptic depression<sup>5, 12, 13</sup>. Despite intensive study of synaptic plasticity, however, the molecular mechanisms underlying spine remodeling associated with LTD, especially long-term maintenance of changes in spines, are still largely unclear.

microRNAs (miRNAs) are short, non-coding RNAs that bind to mRNAs to inhibit translation and/or promote mRNA degradation by imperfect base-pairing between the seed region in miRNAs (usually nucleotides 2–8 at the 5' end) and the miRNA binding site in the 3' untranslated region (3' UTR) of target mRNAs<sup>14</sup>. Each miRNA can potentially target to hundreds of distinct mRNAs, and thousands of genes are regulated by miRNAs. miRNAs are increasingly recognized as key regulators of gene expression and have been found to play important roles in diverse cellular processes, such as the differentiation and development of cells<sup>15, 16</sup>.

miRNAs are crucial for proper brain function. Of the >1000 miRNAs identified in mammals, hundreds are expressed in the brain<sup>17, 18</sup>. miRNA loss in mice due to deficient expression of Dicer or DGCR8, two essential components of the miRNA biogenesis pathway<sup>15</sup>, leads to alterations in synaptic protein expression, synaptic transmission, dendritic spines, learning, and memory<sup>19, 20</sup>. Several miRNAs, such as miR-134, miR-125, miR-138, miR-132, miR-29 and miR-188, regulate the morphogenesis of dendritic spines<sup>16, 21, 22</sup>. The expression of miRNAs is changed during LTP and metabotropic glutamate receptor dependent-LTD, and is regulated by BDNF, which contributes to long-lasting modification of synaptic function<sup>23, 24</sup>. Despite the demonstrated importance of miRNAs, however, the function of the vast majority of miRNAs expressed in the brain have yet to be elucidated, due in part to the limited capacity of traditional experimental techniques and the large number of miRNAs and their target genes. The question of whether or not miRNAs play a role in spine remodeling associated with LTD also remains open.

Here, using next-generation deep sequencing and bioinformatic analyses, we identify miRNAs differentially expressed in hippocampal neurons undergoing LTD, and genes and cellular processes potentially targeted by them. Moreover, by examining the function of

miR-191 (down-regulated) and miR-135 (up-regulated) in hippocampal neurons, we show that both up- and down-regulation of protein synthesis resulting from changes in miRNA transcriptomes are required for persistent and delayed, but not the initiation of spine restructuring in LTD. We demonstrate specifically that miR-191 and miR-135 contribute to spine remodeling by regulating the expression of their target genes tropomodulin 2 and complexin-1/2, respectively. In addition, we find that actin depolymerization and AMPA receptor exocytosis are regulated by miRNAs for prolonged periods of time in long-lasting spine plasticity. This study provides a catalog of miRNAs, genes and cellular processes potentially involved in spine plasticity associated with LTD, demonstrates that miRNAs are crucial regulators of gene expression to orchestrate cellular processes essential for long-lasting structural changes of synapses, and identifies a novel function of AMPA receptor exocytosis in spine plasticity.

## Results

### Changes in the miRNA transcriptome during NMDAR-LTD

To determine whether miRNAs are involved in spine remodeling associated with LTD, we first used next-generation deep sequencing to systematically interrogate the change in miRNA expression following induction of NMDAR-LTD in the mouse hippocampus. To induce LTD, hippocampal slices from mice (17–19 days old) were treated with NMDA (30  $\mu$ M, 5 min). NMDA treatment induces “chemical LTD”, which shares molecular mechanisms with electrical stimulation-induced LTD and causes long-lasting synaptic depression and spine loss in most synapses of the slice<sup>13, 25, 26</sup>. Consistent with reported studies, after NMDA treatment we observed a persistent decrease in field excitatory postsynaptic potentials (fEPSP) of CA1 neurons (mean  $\pm$  SEM: 20.3  $\pm$  4.0% of baseline at 10 min, 55.4  $\pm$  5.4% of baseline at 90 min, 62.3  $\pm$  5.6% of baseline at 2 hr after stimulation; n = 10 slices for each group; Supplementary Fig. 1).

At 90 min after LTD induction, the CA1 region was removed for RNA extraction and preparation of miRNA sequencing libraries. A total of 8 libraries (4 NMDA-treated and 4 sham-treated controls) were sequenced by using an Illumina GAII analyzer. On average, 0.92 million reads were generated from each library, 52.65% of which were mapped to mature miRNAs. From the total 3,660,602 mapped reads, 438 mature miRNAs were identified (Fig. 1a, b). The number of miRNAs detected by our deep sequencing is in line with previous reports that ~300 miRNAs are expressed in the rodent brain<sup>17, 27</sup>.

The fold change and p-value of individual miRNAs are illustrated in Fig. 1. The fold changes are independent on the count of expression tags (Fig. 1a), suggesting that our deep sequencing was unbiased on miRNA abundance. The p-value was computed by controlling the false discovery rate (FDR) for multiple hypothesis testing<sup>28</sup>, and a p-value cutoff of 0.05 was applied to select differentially expressed miRNAs (Fig. 1b). A total of 70 miRNAs were changed in expression after LTD induction (34 up-regulated, 36 down-regulated; Fig. 1a, b).

To validate the deep-sequencing result with an independent assay and preparation, we measured the expression change of several miRNAs in cultured hippocampal neurons using

quantitative real-time PCR (qRT-PCR). Neurons (DIV17) were treated with NMDA (30  $\mu$ M, 5 min) and harvested at 90 min after stimulation for RNA isolation and qRT-PCR. The expression of miR-191 decreased, that of miR-106b, miR-135b, miR-136-3p, miR-19a, miR-19b and miR-466b increased, and that of miR-218, miR-29a, and miR-32 remained unaltered following NMDA treatment (Fig. 1c). The expression level of miR-135a slightly increased, but not to a statistically significant level ( $p = 1.00$ ). These qRT-PCR results are largely consistent with our findings using deep sequencing.

Taken together, these results indicate that following LTD induction the miRNA transcriptome changes substantially, suggesting that miRNAs may play roles in the structural and functional plasticity of synapses.

### Genes and cellular processes targeted by changed miRNAs

miRNAs exert their cellular functions mainly by regulating translation of mRNAs. Each type of miRNA can potentially regulate hundreds of mRNA transcripts, and in most cases, a single mRNA is targeted by multiple miRNA species. To obtain a comprehensive view of the impact of miRNA transcriptome changes on cell physiology, we conducted the miR-gene-gene ontology (GO) enrichment analysis<sup>27</sup> for miRNAs differentially expressed in LTD. To focus on miRNAs that are likely to have significant effects on gene expression, we analyzed only those with read counts > 30 in all samples. Up- and down-regulated miRNAs were analyzed in separate groups. The complete lists of enriched genes and GO terms are shown in Supplementary Data 1 and 2. Some enriched GO terms are related to the regulation of synaptic functions and dendritic spines, such as “synaptic transmission”, “actin filament-based process”, “cytoskeletal protein binding”, “regulation of phosphorylation”, and “small GTPase mediated signal transduction”. These GO terms along with their corresponding miRNAs are illustrated in Supplementary Fig. 2 and Supplementary Data 2. Our findings from these analyses suggest that in neurons undergoing LTD, differentially expressed miRNAs regulate many different cellular processes involved in the structural and functional remodeling of synapses.

### miR-191 and miR-135 regulate prolonged spine remodeling

To examine how altered miRNA expression affects synaptic modification following LTD induction, we conducted time-lapse imaging in cultured hippocampal neurons. In this test, we focused on miR-191 and miR-135, which target to genes and GO terms implicated in the remodeling of dendritic spines and synaptic plasticity. For instance, miR-191 targets tropomodulin 2, which regulates actin dynamics, and the GO terms “cytoskeletal protein binding” and “synaptic transmission”. Likewise, miR-135 targets complexin-1 and -2, which regulate AMPA receptor trafficking, and the GO terms “cytoskeleton organization”, “regulation of MAPK cascade” and “actin filament-based process” (Supplementary Fig. 2, Supplementary Data 1 and 2)<sup>29–32</sup>.

Our deep sequencing shows that while miR-191 is down-regulated, both miR-135a and miR-135b, the two isoforms of miR-135 which target to same genes, are up-regulated after LTD induction. To counteract their changes in expression during LTD, we transfected hippocampal neurons (DIV14) with constructs expressing miR-191 or miR-135 sponge that

sequesters endogenous miR-135a/b and increases the expression of its confirmed targets complexin-1 and -2 (Supplementary Fig. 3a–b and Supplementary Fig. 4c), or antisense oligonucleotides against miR-135a/b. A construct expressing venus (a mutant of YFP)<sup>33</sup> was co-transfected to visualize dendritic spines. At 3–5 days after transfection, neurons were treated with NMDA (30  $\mu$ M, 5 min) for LTD induction. Time-lapse confocal microscopy was used to image the same spines of transfected neurons before and at 10, 30 and 90 min after NMDA treatment. NMDA treatment caused rapid shrinkage of spines. By 10 min after stimulation, spine area was reduced by  $11.2 \pm 3.0\%$  (mean  $\pm$  SEM; n = 8 cells for the sham treated group, n = 15 cells for the NMDA treated group; Fig. 2). The decrease in spine size was progressive and long-lasting. By 90 min after stimulation, spine size was reduced by  $24.5 \pm 3.8\%$  (mean  $\pm$  SEM; n = 9 cells for the sham treated group, n = 16 cells for the NMDA treated group), and more spines were retracted (Fig. 2).

In cells transfected with the miR-191 construct, the miR-135 sponge construct or antisense oligonucleotides against miR-135, NMDA-induced spine shrinkage at 10 min post-stimulation was comparable to that in control cells (Fig. 2, Supplementary Fig. 3c, d). However, spine size gradually recovered thereafter, and was indistinguishable from sham-treated cells by 30 min after stimulation (Fig. 2, Supplementary Fig. 3c, d). The increase in spine retraction was also abolished by transfection with the miR-191 construct, miR-135 sponge or miR-135 antisense oligonucleotides (Fig. 2, Supplementary Fig. 3c, d).

We also transfected neurons with a construct expressing miR-32, whose expression was unaffected by NMDA treatment (Fig. 1), or with scrambled miR-135 oligonucleotides. Neither the size of spines, nor NMDA-induced spine shrinkage and retraction were affected by transfection of the miR-32 construct or scrambled oligonucleotides (Fig. 2, Supplementary Fig. 3c, d). In addition, without NMDA treatment, the size and density of dendritic spines were unaffected by transfection of the miR-191 construct, miR-135 sponge, miR-135 antisense oligonucleotide or the miR-32 construct (Supplementary Fig. 3e). These results suggest that the effect of miR-191, miR-135 sponge or antisense oligonucleotides on NMDA-induced spine plasticity is not due to non-specific changes in cell physiology.

Taken together, these results indicate that miR-191 inhibits, while miR-135 promotes NMDA-induced spine retraction and long-lasting spine shrinkage, and therefore suggest that their expression changes in LTD are required for prolonged spine remodeling.

### Spine remodeling in LTD is translation-dependent

As the main function of miRNAs is translational regulation, our findings on miR-191 and miR-135 suggest that protein synthesis might be involved in modification of spines during LTD. To test this possibility, we tested the effects of the translational inhibitors anisomycin and emetine on NMDA-induced spine remodeling. Prior to NMDA treatment, anisomycin (20  $\mu$ M) and emetine (20  $\mu$ M) were added to the bath solution of neurons transfected with a construct expressing venus. In inhibitor-treated cells, spine size was reduced at 10 min post-stimulation with NMDA, but by 30 and 90 min after stimulation, it is comparable to that in sham-treated cells (Fig. 2, Supplementary Fig. 3c, d). The two translational inhibitors also abolished NMDA-induced spine retraction (Fig. 2, Supplementary Fig. 3c, d). By contrast, the transcriptional inhibitor actinomycin D (10  $\mu$ M) had no effects on NMDA-induced spine

shrinkage or retraction (Supplementary Fig. 3c, d). These results indicate that translation, but not transcription, is required for NMDA-induced spine elimination and persistent reduction in spine size.

### **Tropomodulin 2 is miR-191's target and up-regulated in LTD**

To determine how miR-191 regulates spine remodeling, we looked into its target genes. Among miR-191's predicted targets, tropomodulin 2 (Tmod2) has two predicted miR-191-binding sites in its 3'UTR and the most total favorable context score for miR-191 recognition<sup>34, 35</sup>. Moreover, based on our miR-gene-GO enrichment analysis, some GO terms targeted by Tmod2, such as "cytoskeletal protein binding", are closely related to spine remodeling (Supplementary Fig. 2, 5a, Supplementary Data 2). Hence, we tested whether Tmod2 mediates the effect of miR-191 on spine plasticity associated with LTD.

First, we tested whether Tmod2 is a true target of miR-191. We generated a reporter construct by inserting the 3'UTR of Tmod2 behind the destabilized mCherry sequence. This reporter construct was transfected into cultured hippocampal neurons (DIV14) along with a plasmid expressing both EGFP and miR-191. At 3 days after transfection, mCherry expression was assessed by measuring the intensity ratio of fluorescence produced by mCherry and EGFP. The expression of mCherry by the reporter construct was greatly reduced by co-transfection with the miR-191 construct, but not a construct expressing miR-135b which is not predicted to interact with Tmod2, or an EGFP construct expressing no miR-191 (Fig. 3a, b). To test whether miR-191 represses mCherry expression through the miR-191 binding sites in the 3'UTR of Tmod2, we mutated the miR-191 binding sites in the reporter construct, and found that mCherry expression by the mutated reporter construct was no longer affected by transfection of the miR-191 plasmid (Fig. 3a, b). These results indicate that the 3'UTR of Tmod2 confers translational control by miR-191.

To test whether miR-191 also regulates endogenous Tmod2 expression, cultured cortical neurons were transduced with lentivirus expressing miR-191, or transfected with antisense oligonucleotides against miR-191. Tmod2 expression was analyzed by immunoblotting. The miR-191 virus reduced, while antisense oligonucleotides increased Tmod2 expression (Fig. 3c, d and Supplementary Fig. 4a). These results confirm that Tmod2 is a physiological target of miR-191.

Next, we tested whether Tmod2 expression is changed during LTD. Cultured hippocampal neurons were treated with NMDA (30  $\mu$ M, 5 min), and stained with the Tmod2 antibody at 90 min after stimulation. In cells transfected with the control plasmid, NMDA treatment caused an increase in Tmod2 expression, and this increase was induced at the translational but not transcriptional level, as the translational inhibitor anisomycin inhibited it, but the transcriptional inhibitor did not (Fig. 3e, f). To test whether miR-191 contributes to the change in Tmod2 expression, we transfected neurons with the miR-191 construct to compensate for NMDA-induced reduction in miR-191 expression. miR-191 transfection abolished NMDA-induced changes in Tmod2 expression (Fig. 3e, f). These data indicate that NMDA-induced decreases in miR-191 expression results in enhanced expression of Tmod2.

Taken together, these findings indicate that Tmod2 is a physiological target of miR-191 and that reduced miR-191 expression during LTD leads to increased expression of Tmod2.

### **Tmod2 is essential for spine plasticity associated with LTD**

Having demonstrated that Tmod2 is a target of miR-191 and is up-regulated following LTD induction, we next examined its role in spine plasticity. To this end, we generated a construct expressing siRNAs against Tmod2. The efficacy and specificity of Tmod2 siRNAs were tested against exogenously and endogenously expressed Tmod2 in COS-7 cells and primary hippocampal neurons, respectively (Supplementary Fig. 5b–e and Supplementary Fig. 4d). Cultured hippocampal neurons (DIV14) were transfected with the highly effective and specific Tmod2 siRNA (siRNA-4), treated with NMDA (30  $\mu$ M, 5 min), and imaged before and after NMDA treatment. As measured at 10, 30, and 90 min after NMDA stimulation, the size of spines and the number of eliminated spines in Tmod2 siRNA transfected and sham treated neurons were comparable (Fig. 4). Transfection of the Tmod2 siRNA construct did not change the basal level of spine size or density (Supplementary Fig. 5f, g). These results indicate that Tmod2 is required for NMDA-induced spine shrinkage and elimination.

To test whether Tmod2 mediates miR-191 function in LTD, we transfected hippocampal neurons (DIV14) with the miR-191 expressing construct along with a construct expressing Tmod2, and stimulated these cells with NMDA (30  $\mu$ M, 5 min) at 3 days after transfection. The size and density of spines were not changed by co-transfection of the Tmod2 siRNA and the miR-191 construct (Supplementary Fig. 5f, g). While long-lasting spine shrinkage and spine elimination induced by NMDA treatment were both blocked in miR-191 transfected cells (Fig. 2), co-transfection of the Tmod2 with the miR-191 construct restored these changes (Fig. 4). These results indicate that miR-191 restricts spine plasticity by limiting the expression of Tmod2.

To test whether other miR-191 target genes also regulate spine remodeling, we co-transfected hippocampal neurons (DIV14) with the miR-191 construct and a construct expressing EGR1 (a reported miR-191 target)<sup>36</sup>. NMDA-induced spine shrinkage and elimination were indistinguishable in miR-191 and EGR1 co-transfected and miR-191 overexpressing cells (Supplementary Fig. 6). Hence, unlike Tmod2, EGR1 does not contribute to the function of miR-191 in NMDA-induced spine remodeling.

Taken together, these findings indicate that in LTD increased Tmod2 expression resulting from a reduction in miR-191 is required to maintain spine changes.

### **Tmod2 modifies actin filaments in LTD**

Tmod2 is a neuron-specific member of the tropomodulin family<sup>37</sup>. Tropomodulins are actin filament pointed end-capping proteins which regulate the dynamics, length and amount of actin filaments (F-actin)<sup>29</sup>. Since actin depolymerization is promoted by LTD induction and underlies spine shrinkage<sup>5, 31</sup>, Tmod2 may also play a role in actin regulation during LTD. To test this possibility, we transfected cultured hippocampal neuron (DIV14) with a construct expressing the Tmod2 siRNA construct, and stained F-actin with phalloidin. In neurons transfected with the control plasmid, NMDA treatment caused a reduction in the F-

actin content (Fig. 5). Tmod2 siRNA transfected cells, however, contained comparable levels of F-actin, whether or not they were treated with NMDA (Fig. 5). Likewise, transfection of the miR-191 construct also blocked NMDA-induced F-actin change (Fig. 5), and this effect of miR-191 was obliterated by co-transfection with a construct expressing Tmod2 (Fig. 5). By contrast, transfection with the miR-135b construct or miR-135 antisense oligonucleotides had no effect on NMDA-induced F-actin reduction (Fig. 5). These results indicate that Tmod2 is required for NMDA-induced actin reorganization and for the effect of miR-191 down-regulation on F-actin.

### miR-135 regulates complexin-1/2 for spine remodeling in LTD

miR-135 targets both complexin-1 and -2 (Supplementary Fig. 3a, b and Supplementary Fig. 4c), which are 86% identical at the amino acid level in rats and perform redundant functions<sup>38</sup>. In addition, our miR-gene-GO enrichment analysis found that complexin-1 and -2 are annotated by GO terms related to spine morphogenesis, such as “nervous system development” (Supplementary Data 2, Supplementary Fig. 5a), suggesting that they might be involved in spine plasticity. Hence, we tested whether complexins mediate the promoting effect of miR-135 on spine remodeling during LTD.

If complexins are, in fact, miR-135 effectors in LTD, it is likely that NMDA treatment will alter complexin expression. To test this possibility, we treated cultured cortical neurons (DIV17) with NMDA (30  $\mu$ M, 5 min) and assessed complexin expression by immunoblotting with an antibody against both complexin-1 and -2. The expression of both complexin-1 and complexin-2 was decreased by NMDA treatment, and this decrease was abolished by transfection with the miR-135 antisense oligonucleotides prior to NMDA treatment (Fig. 6a, b and Supplementary Fig. 4b). These results indicate that by up-regulating miR-135, NMDA treatment decreases the expression of complexin-1 and -2.

To test whether the expression change of complexins is required for spine remodeling, we transfected hippocampal neurons (DIV14) with the venus construct along with a construct expressing complexin-1 to compensate for diminished complexin expression induced by NMDA treatment. At all examined time points after NMDA stimulation, spine size and elimination were comparable in complexin-1 transfected cells and sham-treated controls (Fig. 6c–e). Transfection of the complexin-1 construct left the basal level of spine size and density intact (Supplementary Fig. 7a, b). These results indicate that the reduction in complexin expression is required for NMDA-induced spine shrinkage and elimination.

To test whether complexins mediate the effect of miR-135 on spine remodeling, we transfected hippocampal neurons (DIV14) with a construct expressing siRNAs against both complexin-1 and -2 (Supplementary Fig. 7c, d and Supplementary Fig. 4e) along with the miR-135 sponge construct or miR-135 antisense oligonucleotides. Co-transfection of the complexin-1 construct and the miR-135 sponge construct or miR-135 antisense oligonucleotides did not change the baseline of spine size and density (Supplementary Fig. 7a, b). While NMDA-induced spine elimination and long-lasting spine shrinkage were blocked by miR-135 sponge or antisense oligonucleotides (Fig. 2, Supplementary Fig. 8), these changes were restored in cells co-transfected with the complexin siRNA construct and miR-135 sponge or antisense oligonucleotides (Fig. 6c–e, Supplementary Fig. 8). These



results show that regulation of complexin expression by miR-135 promotes spine remodeling.

To test whether other miR-135 targets also contribute to NMDA-induced spine remodeling, we co-transfected hippocampal neurons (DIV14) with the miR-135 sponge construct and a construct expressing siRNAs against Rap2, which is also a target gene of miR-135 (Supplementary Fig. 3a, b and 7e, f and Supplementary Fig. 4c, f). Transfection of the Rap2 siRNA construct left the effect of miR-135 sponge on NMDA-induced spine shrinkage and elimination unchanged (Supplementary Fig. 8), indicating that Rap2 does not mediate the function of miR-135 in spine remodeling.

Taken together, these results indicate that complexin-1 and -2 are the targets of miR-135 responsible for its function in NMDA-induced spine remodeling.

### Reduced complexin expression alters AMPA receptor exocytosis

Complexin-1 and -2 are SNARE-complex binding proteins and regulate both pre- and postsynaptic exocytosis<sup>30, 39</sup>. Although the role of postsynaptic exocytosis in LTD has yet to be examined, it has been shown to regulate spine size during LTP<sup>40</sup>. To determine the mechanism by which complexin contributes to spine remodeling, we explored the possibility that complexins regulate postsynaptic exocytosis in LTD. First, we tested whether LTD induction alters dendritic exocytosis. Exocytosis of postsynaptic membrane was assessed by monitoring exocytosis of the AMPA receptor subunit GluA1 using fluorescence recovery after photobleaching (FRAP). Cultured hippocampal neurons (DIV14) were transfected with a DsRed construct (for visualization of neuronal morphology) along with a construct expressing GluA1 tagged with a pH-sensitive form of EGFP (Super Ecliptic pHluorin, SEP) that displays fluorescence only when it is present on the cell surface<sup>41–43</sup>. At 3–5 days after transfection, neurons were treated with NMDA (30  $\mu$ M, 5 min). At 30 min after NMDA treatment, a small dendritic segment (25–30  $\mu$ m) was photobleached to eliminate > 95% SEP fluorescence, and images were taken every 2–10 min thereafter. After photobleaching, SEP fluorescence in sham-treated neurons gradually recovered, with a recovery time constant ( $\tau$ ) of  $21.6 \pm 3.0$  min (mean  $\pm$  SEM,  $n = 12$  cells; Fig. 7). By contrast, NMDA treatment greatly slowed GluA1 recovery after photobleaching ( $\tau = 105.2 \pm 11.8$  min, mean  $\pm$  SEM,  $n = 7$  cells,  $p = 0.00008$  vs. sham-treated controls, U test; Fig. 7). These results indicate that AMPA receptor exocytosis is inhibited by NMDA treatment.

To test whether miR-135 plays a role in changing AMPA receptor exocytosis, we transfected hippocampal neurons (DIV14) with the miR-135 sponge construct or miR-135 antisense oligonucleotides to counteract NMDA-induced up-regulation of miR-135, then measured GluA1 exocytosis. After NMDA treatment, GluA1 exocytosis occurred faster in sponge ( $\tau = 22.3 \pm 2.4$  min, mean  $\pm$  SEM,  $n = 6$  cells,  $p = 0.0082$  vs. NMDA-treated controls, U test; Fig. 7) or antisense oligonucleotides ( $\tau = 21.3 \pm 2.4$  min, mean  $\pm$  SEM,  $n = 10$  cells,  $p = 0.0004$  vs. NMDA-treated controls, U test; Supplementary Fig. 9) transfected cells than in control plasmid-transfected cells. These results indicate that miR-135 inhibits postsynaptic exocytosis following NMDA treatment.

Next, we tested whether complexins contribute to NMDA-induced retardation of exocytosis. Hippocampal neurons (DIV14) were transfected with a complexin-1 expressing construct, and treated with NMDA (30  $\mu$ M, 5 min) at 3–5 days after transfection. GluA1 exocytosis was measured at 30 min after NMDA treatment using FRAP. In the complexin-1 construct transfected cells, the recovery of GluA1 after photobleaching was faster than in control plasmid transfected cells, and comparable to that in sham treated cells ( $\tau = 30.2 \pm 2.8$  min, mean  $\pm$  SEM,  $n = 8$  cells,  $p = 0.0006$  vs. NMDA-treated controls;  $p = 0.12$  vs. sham-treated cells, U test; Fig. 7), indicating that reduced complexin expression induced by NMDA treatment slows GluA1 exocytosis.

To test whether the effect of miR-135 on GluA1 exocytosis is mediated by complexins, we transfected hippocampal neurons with the complexin siRNA construct along with the miR-135 sponge construct or miR-135 antisense oligonucleotides. In the co-transfected cells, GluA1 exocytosis after NMDA treatment was far less than in cells transfected with the miR-135 sponge construct or miR-135 antisense oligonucleotides alone, and comparable to that in NMDA-treated controls (Fig. 7, Supplementary Fig. 9). By contrast, basal GluA1 exocytosis without NMDA treatment was not affected by miR-135 or complexin-1 (Supplementary Fig. 10). These results indicate that miR-135 regulates AMPA receptor exocytosis in NMDA treated neurons by suppressing complexin expression.

Taken together, these results indicate that postsynaptic exocytosis was decreased by NMDA treatment, and that this decrease is attributable to repression of complexin expression by miR-135.

### miR-191 and miR-135 are essential for LTD induction

Having delineated the function of miR-191 and miR-135 in spine plasticity associated with LTD, we proceeded to test whether they also play roles in the depression of synaptic transmission. Cultured hippocampal slices were transduced with lentivirus expressing miR-191 or miR-135 sponge. At 5 days after transduction, LTD was induced in the CA1 region by stimulating the Schaffer collateral pathway (1Hz, 15 min). In control virus transduced cells, fEPSPs were decreased by the stimulation (mean  $\pm$  SEM: 68.9  $\pm$  2.0% of baseline at 10 min, 64.7  $\pm$  6.1% of baseline at 90 min, and 62.7  $\pm$  4.3% of baseline at 2 hr after stimulation;  $n = 6$  slices; Fig. 9). By contrast, LTD was greatly reduced in cells transduced with the miR-191 or miR-135 sponge virus [mean  $\pm$  SEM: 91.5  $\pm$  7.0% ( $p = 0.041$  vs. control), 101.0  $\pm$  4.9% ( $p = 0.0021$  vs. control), 101.0  $\pm$  6.4% ( $p = 0.0043$  vs. control), and 95.7  $\pm$  7.4% ( $p = 0.0043$  vs. control) of baseline for miR-191; 81.9  $\pm$  3.0% ( $p = 0.0022$  vs. control), 88.0  $\pm$  2.8% ( $p = 0.026$  vs. control), 93.5  $\pm$  6.7% ( $p = 0.0087$  vs. control), and 87.5  $\pm$  2.8% ( $p = 0.0022$  vs. control) of baseline for miR-135 at 10, 30, 90, and 120 min post-stimulation, respectively.  $n = 6$  slices for each group, U test; Fig. 8]. These results indicate that the induction of LTD requires proper expression levels of miR-191 and miR-135.

### Both pri- and mature miR-191 and miR-135b are changed in LTD

To explore the mechanisms by which miR-191 and miR-135 are changed in LTD, we assessed the levels of pri- and mature miR-191 and miR-135b at various time points after

NMDA treatment. Hippocampal neurons (DIV17) were treated with NMDA (30  $\mu$ M, 5 min), and harvested at 10, 30, 60 and 90 min after NMDA stimulation. Pri- and mature miRNAs were analyzed using qRT-PCR. The expression of both mature and pri-miR-191 was reduced by NMDA treatment (Fig. 9a). Likewise, both mature and pri-miR-135b were changed by NMDA treatment (Fig. 9b). The elevation of mature and pri-miR-135b, however, started earlier than the decrease in mature and pri-miR-191 (Fig. 9a, b), suggesting that the expression changes in these two miRNAs might be induced by different mechanisms.

The changes in the pri form of miR-191 and miR-135b after LTD induction indicate that these miRNAs are regulated at the transcriptional level. To test whether they are also regulated at post-transcriptional levels in LTD, we treated hippocampal neurons (DIV17) with the transcriptional inhibitor actinomycin D (10  $\mu$ M) along with NMDA. Despite the presence of actinomycin D, NMDA treatment still altered the levels of mature miR-191 and miR-135b (Fig. 9c), suggesting that post-transcriptional processing of these miRNAs are also regulated by NMDA treatment.

To test whether NMDA-induced changes in miRNAs have impact on miRNAs incorporated into RISC, we analyzed miR-191 and miR-135b associated with RISC by using the cross-linking and immunoprecipitation (CLIP) assay. We transduced primary cortical neurons with lentivirus expressing Flag-tagged argonoute 2 (Ago2, a protein component of RISC). At 10 days after transduction, RISC in transduced neurons was cross-linked by UV irradiation, and then pulled down with an anti-Flag antibody. miRNAs in immunoprecipitated RISC were measured by qRT-PCR using miR-218 and miR-29a (two miRNAs unaffected by NMDA treatment, Fig. 1) as controls. We found that the level of miRNA-191 in RISC was decreased, and that of miR-135b was increased (Fig. 9d)

Taken together, these results indicate that in LTD, miR-191 and miR-135b are regulated at both transcriptional and post-transcriptional levels.

### **NMDA treatment alters dendritic miR-191 and miR-135b**

Several miRNAs and RISC proteins are found in dendrites where they could locally regulate translation<sup>44</sup>. To test whether miR-191 and miR-135b are localized in dendrites, we assessed their subcellular distribution by using *in situ* hybridization (ISH). Hippocampal neurons (DIV14) were transfected with the EGFP construct for visualization of dendrites. At 3 days after transfection, locked nucleic acid (LNA) probes were used for miRNA ISH. miR-191 and miR-135b were detected in both soma and dendrites (Fig. 10a). By contrast, the signals of a control probe for the U6 small nuclear RNA were found mainly in the soma, and those of another control probe for miR-215 (which is expressed at a negligible level in hippocampal neurons based on our deep-sequencing analysis) were little (Fig. 10a), confirming the specificity of our ISH assay. These results indicate that miR-191 and miR-135b are indeed localized in dendrites.

To test whether dendritic miR-191 and miR-135b are changed in LTD, we treated hippocampal neurons (DIV17, 3 days after transfection with the EGFP construct) with

NMDA (30  $\mu$ M, 5 min). At 90 min after treatment, neurons were fixed for ISH. Notably, miR-191 and miR-135b in dendrites were altered by NMDA treatment (Fig. 10b–d).

To test whether dendritic miR-191 and miR-135b can be regulated locally in LTD, we treated hippocampal neurons with NMDA along with actinomycin D (10  $\mu$ M) to block transcription, and the actin polymerization inhibitor cytochalasin D (10  $\mu$ M) or the microtubule polymerization inhibitor nocodazole (10  $\mu$ M) to interfere with intracellular transportation of miRNAs. Dendritic miR-191 and miR-135b were still changed by NMDA treatment when transcription and intracellular trafficking were inhibited (Fig. 10b–d). Hence, NMDA treatment can regulate miR-191 and miR-135b locally in dendrites.

The dendritic localization of miRNA-191 and miR-135b suggests that they might regulate the expression of their target mRNAs in dendrites. To test this possibility, we first assessed the subcellular localization of Tmod2 and complexin-1 mRNAs. Our ISH assay showed that both Tmod2 and complexin-1 mRNAs were indeed localized in dendrites (Supplementary Fig. 11a). We then tested whether expression of dendritic Tmod2 and complexin-1 were altered in LTD by blocking transcription and intracellular trafficking with actinomycin D, cytochalasin D and nocodazole. Despite the presence of these inhibitors, the expression of both dendritic Tmod2 and complexin-1 and -2 was changed by NMDA treatment (Supplementary Fig. 11b–e). These results indicate that the expression of Tmod2 and complexins can be regulated locally in dendrites during LTD.

Taken together, these findings indicate that in LTD, the expression changes in miR-191, miR-135b and their targets are caused at least in part by local miRNA processing and translation in dendrites.

### **Different NMDAR subunits regulate miR-191 and miR-135b**

Having demonstrated the importance of miRNAs in NMDAR-LTD, we went on to test the role played by NMDA receptors in the regulation of miRNAs. We treated hippocampal neurons (DIV17) with NMDA (30  $\mu$ M, 5 min) along with the NMDAR antagonist AP5 [(2*R*)-amino-5-phosphonovaleric acid, 100  $\mu$ M], and isolated RNA at 90 min after treatment for qRT-PCR analysis of miRNAs. The changes in miR-191 and miR-135b induced by NMDA treatment were blocked by AP5. Hence, NMDAR is essential for the regulation of miRNAs in LTD (Fig. 10e).

In hippocampal neurons, NMDAR is composed of GluN1 and GluN2 subunits (GluN2A and GluN2B)<sup>45</sup>. GluN1 is an obligate subunit, while GluN2A and GluN2B have different functions. To test which GluN2 subunit regulates miRNAs in LTD, we treated hippocampal neurons (DIV17) with NMDA (30  $\mu$ M, 5 min) along with the GluN2A antagonist TCN 201 (10  $\mu$ M) or GluN2B antagonists Ro 25-6891 (3  $\mu$ M), and isolated RNA at 90 min after treatment. Notably, after NMDA stimulation, the decrease in miR-191 was blocked by GluN2B antagonists (but not the GluN2A antagonist), while the increase in miR-135 was blocked by the GluN2A antagonist (but not GluN2B antagonists) (Fig. 10e). By contrast, the AMPA receptor blocker NBQX (2,3-Dioxo-6-nitro-1,2,3,4-tetrahydrobenzo[*f*]quinoxaline-7-sulfonamide, 10  $\mu$ M) had no effect on NMDA-induced changes in miR-191 and miR-135b (Fig. 10e).

Taken together, these results indicate that NMDAR is required for the change in miRNA expression associated with LTD, and that GluN2A and GluN2B play different roles in the regulation of miRNAs.

## Discussion

In this study, we examined the role of miRNAs in the structural plasticity of dendritic spines in LTD. Using deep sequencing to profile the miRNA transcriptome, we compiled a comprehensive list of miRNAs differentially expressed in LTD. We also employed both computational and experimental approaches to investigate cellular processes regulated by these miRNAs. Our results show that a large number of miRNAs, affecting many different cellular processes, are altered in expression by LTD induction. With live imaging and electrophysiology, we demonstrated experimentally that miR-191 and miR-135 are essential for sustained spine remodeling and induction of synaptic depression in LTD. We also identified the genes and cellular processes targeted by these two miRNAs to modulate spines.

While several miRNAs have been shown to regulate dendritic spine morphology, the role of miRNAs in spine plasticity has yet to be examined. Investigation of this question is to some extent hampered by the large number of miRNAs. We tackled this problem by using deep sequencing to screen for candidate miRNAs involved in LTD. The next-generation sequencing technologies have significantly pushed back the limitations of prior transcriptome profiling approaches by greatly improving the throughput, depth of coverage, sensitivity, and quantifiability. They are particularly advantageous when analyzing miRNAs expressed in the brain, many of which are low- to moderate-abundance transcripts.

Our deep-sequencing results reveal notable changes, in both directions, in the miRNA transcriptomes of neurons undergoing LTD. Down-regulation of miRNAs is expected to enhance, while the increase in miRNA levels is predicted to suppress translation. Hence, the alteration in miRNA transcriptomes suggests that miRNAs contribute to the bidirectional change of gene expression in LTD.

Our findings that a large number of miRNAs are changed in expression after NMDA treatment is in accordance with previous reports that activation of NMDA or metabotropic glutamate receptors has notable effects on miRNA expression<sup>23, 46, 47</sup>. In particular, several miRNAs including miR-191, miR-320, miR-106b, miR-203 and miR-21 are identified as differentially expressed miRNAs in both our and the Kye studies that stimulate neurons with NMDA<sup>46</sup>. Although in the Kye study, the change in miR-135 expression dose not reach a statistically significant level, it shows a trend of increase which is in the same direction as observed in our study. The incomplete overlap in results between our and the Kye study might stem from the differences in cell types and miRNA profiling methods used in the two studies (cultured hippocampal neurons containing all hippocampal regions and quantitative PCR in the Kye study vs. the CA1 region from acute hippocampal slices and deep-sequencing in our study).

We experimentally confirmed that the change in miRNA expression can lead to both increases and decreases in gene expression. For instance, the target of miR-191, *Tmod2*, is increased, while the targets of miR-135, *complexin-1* and *-2*, are decreased as a consequence of miRNA change. Down-regulation of miRNAs is consistent with the accepted notion that the maintenance of synaptic depression is dependent on new protein synthesis<sup>48–50</sup>, and our results that translation is required for long-term stabilization of spine remodeling. Our findings of up-regulated miRNAs, however, reveal unexpectedly a new dimension of proteome regulation in LTD — translational inhibition. Importantly, our functional characterization of miR-191 and miR-135 confirms that bi-directional modulation of protein synthesis is essential for spine plasticity.

To gain a systematic view of the physiological effects of miRNA transcriptome changes, we used a bioinformatic method, which combines a statistical analysis developed in house with publicly available computational and experimental data on miRNA targets and gene functions, to predict miRNA targets and cellular processes that are likely to be regulated by differentially expressed miRNAs. This approach facilitates the selection and prioritization of miRNA targets and cellular activities for experimental validation. Results from this analysis suggest that differentially expressed miRNAs regulate a broad range of activities, and that multiple miRNAs might influence the same cellular process concertedly by targeting to its different components.

Dendritic spines are actin-rich structures. Actin cytoskeleton is essential to sculpt the shape of spines, and its dynamic rearrangement induced by synaptic activity underlies structural remodeling of spines<sup>31</sup>. LTD-inducing stimulations cause a shift of actin from filamentous actin (F-actin) to globular actin (G-actin) in minutes, and F-actin reduction is required for spine shrinkage<sup>5,51</sup>. Activation of the F-actin severing protein cofilin by dephosphorylation and inactivation of the actin polymerization regulator Arp2/3 complex by protein interaction have been implicated as crucial signaling cascades underlying actin reorganization for spine shrinkage in LTD<sup>52,53</sup>. Our findings indicate that the maintenance of F-actin reduction beyond initial spine shrinkage is required to support long-lasting spine remodeling, and that doing so requires the up-regulation of *Tmod2* by miR-191.

AMPA receptor trafficking to and away from postsynaptic membrane is critical for synaptic plasticity<sup>54–56</sup>. In LTD, however, although AMPA receptor endocytosis is a major mechanism of synaptic depression, it is not required for spine shrinkage<sup>12,13</sup>. Surprisingly, we found that to stabilize spine shrinkage in LTD, AMPA receptor exocytosis, which is an important means of enhancing synaptic strength in LTP<sup>57–60</sup>, is inhibited due to miR-135 mediated suppression of *complexin* expression. *Complexin* has been indicated in AMPA receptor exocytosis in LTP. The fact that *complexin* regulates AMPA receptor exocytosis in both LTD and LTP is consistent with the reported interaction between the LTD and LTP pathways<sup>54,55</sup>.

Our findings that *Tmod2* and *complexin-1* and *2* are involved in both spine shrinkage and elimination in LTD suggest that these two processes are controlled by overlapping pathways. This model is consistent with the scenario that excessive spine shrinkage can result in spine loss.

Our analysis of pri-mRNAs indicates that transcriptional regulation contributes to NMDA-induced changes in mature miRNAs. By using ISH to detect the subcellular localization of miRNAs and blocking transcription and intracellular trafficking, we demonstrated that in LTD, miRNAs can also be regulated at post-transcriptional levels locally in dendrites, consistent with the previous report that pre-miRNAs are indeed localized, and therefore presumably processed, in dendrites<sup>61</sup>. It is conceivable that the dendritic localization of miRNA processing machinery and its regulation by synaptic transmission allow timely and spatially restricted control of miRNA levels near synapses, thereby facilitating the specificity and efficiency of synaptic activities. Interestingly, both down-regulation of miR-191 and up-regulation of miR-135b in LTD require NMDAR activity, but are mediated by different GluN2 subunits. It is possible that activation of GluN2A and GluN2B subunits has opposing effects on miRNA biogenesis and/or processing, thereby leading to bidirectional changes in the miRNA transcriptome. Finally, how do cells benefit from using miRNAs to control spine plasticity? While new protein synthesis is required for many forms of synaptic plasticity, such as LTP, LTD and homeostatic synaptic plasticity<sup>62–64</sup>, different types of synaptic plasticity entail distinct changes in synaptic structure and function. For instance, LTD is characterized by synaptic depression and spine shrinkage, while LTP, its functional opposite, features synaptic potentiation and spine enlargement. Because of their large varieties and base-pairing interaction with mRNAs, miRNAs are well positioned to provide transcript- and stimulation-specific fine-tuning of translation. It is conceivable that combination of gene-specific regulatory mechanisms, such as that dependent on miRNAs, with global translational regulation which has been indicated in synaptic plasticity<sup>64</sup>, can efficiently and precisely modulate the proteome to suit the unique needs of each kind of synaptic plasticity.

## Methods

### Animals

17–19-day-old male C57BL/6 mice were used for deep-sequencing, Sprague Dawley rat embryos of 18–19 days old were used for neuronal cultures, and 6–8-day-old Sprague Dawley rats were used for slice cultures. All animal procedures followed the US National Institutes of Health guidelines Using Animals in Intramural Research and were approved by the National Institute of Mental Health Animal Care and Use Committee.

### DNA constructs and reagents

To generate constructs expressing miRNAs, rat pre-miR-135a (primers: GAAATGGTTTTGAAGTCGT and CGTTCCAGAGGCTCTAGTT) and -b (primers: TTCCTCAGTTTCCTGCTCT, and CTCTGTGGCTGGTCCTTAG) and pre-miR-191 (primers: GATGGGCGGGTTCCGGTTT and TGGCCCAGTAGTGTCTGA) were amplified from genomic DNAs by PCR and cloned into the BglIII/HindIII site of the pGSuper vector. The siRNA constructs was made by inserting annealed oligos containing the siRNA sequence against Tmod2 (GGTCAACAAGACCTTGAAA), Complexin-1 and -2 (GGACATGTTCAAGAAGTAA) into the pSuper vector. The cDNAs of Tmod2 and complexin-1 were obtained by RT-PCR and cloned into the GW1 vector. To generate the reporter construct, the 3'UTR of Tmod2 was amplified from rat brain cDNA by PCR and

cloned into the pCMV-mCherry-Ds vector behind the mCherry sequence. The miR-191 precursor along with the H1 promoter was amplified from the miR-191-pGsuper construct by PCR (using primers: GCTGCAGGAATTCGAACG and GGTGAGCAAAAACAGGAAGG) and cloned into the pRRLsin.CMV.GFPpre vector for lentivirus production. The miRNA binding sites in the miR-135 and the miR-215 sponge were designed as reported<sup>65</sup> (miR-135: TCACATAGGAATTTAAGCCATA; miR-215: TGTCTGTCAAAGTTAGGTCAT). 10 miRNA binding sites were inserted into the 3' UTR region of EGFP in the pRRLsin.CMV.GFPpre vector for production of lentivirus. The following constructs were obtained as gifts: GluR1-SEP (Bo Li, Cold Spring Harbor Laboratory), pRRLsin.CMV.GFPpre (Scott Young, National Institute of Mental Health, National Institutes of Health). The following reagents were obtained commercially: miR-135 and miR-191 antisense oligonucleotide (IDT), NMDA (Sigma-Aldrich), anisomycin (Sigma-Aldrich), Emetine (Sigma-Aldrich), actinomycin D (Sigma-Aldrich), AP5 (Sigma-Aldrich), Ro 25-6891 (Sigma-Aldrich), TCN 201 (Tocris), Cytochalasin (Sigma-Aldrich), Nocodazole (Sigma-Aldrich), NBQX (Sigma-Aldrich), the COS-7 cell line (ATCC), anti-Tmod2 (1:200 for immunocytochemistry and 1:3000 for western blot, Abcam, Cat # ab67407), anti-complexin-1 and -2 antibody (1:500 for immunocytochemistry and 1:3000 for western blot, Synaptic Systems, Cat # 122002), anti-HA antibody (1:1000, Covance, Cat # MMS-101P), anti-Myc antibody (1:1000, CalBiochem, Cat # OP10), anti-digoxigenin-POD antibody (1:100, Roche, Cat # 11207733910) and anti-actin antibody (1:5000, Sigma-Aldrich, Cat # A4700).

### Construction of miRNA sequencing libraries and deep sequencing

CA1 regions of mouse hippocampi were removed and homogenized with a Polytron homogenizer (Kinematica) in the lysis buffer provided by the mirVana miRNA Isolation Kit (Ambion). The lysate was extracted with acid-phenol:chloroform, added ethanol to bring up the sample to 25% ethanol and fractionated to isolate the large and small RNAs by using the glass-fiber filter of mirVana miRNA Isolation Kit. RNA integrity number (RIN) of the extracted RNA samples was measured to assess RNA quality by using the Agilent 2100 Bioanalyzer. miRNAs were purified from the small RNA fraction by using denaturing polyacrylamide gel electrophoresis (15%) followed by recovering the 17~27-nt-long RNA fragments which were enriched for miRNAs. Deep-sequencing libraries were constructed by using the Small RNA Sample Prep kit (Illumina). Briefly, 3' adaptors and 5' adaptors were ligated to purified miRNAs sequentially. Adaptor tagged miRNAs were reverse-transcribed and amplified by low-cycle PCR. The PCR products were purified by polyacrylamide gel electrophoresis (8%) and sequenced using an Illumina Genome Analyzer II.

### Deep-sequencing data analysis

Sequence data analysis was performed as previously described<sup>27</sup>. Briefly, raw sequence reads were first consolidated by clustering identical sequence reads. Only reads containing complete 3' and 5' adaptor sequences were subjected to downstream analysis. After trimming of 3' and 5' adaptor sequences, the remaining sequences were aligned to miRNA hairpin sequences downloaded from the miRBase database (<http://www.mirbase.org/>) by using Bowtie v0.2.1<sup>66</sup>. Mappable reads were further filtered to remove those that do not map to mature miRNAs. The expression count of each miRNA (≥ 5 read counts in at least



50% samples) was normalized to the total number of mapped reads of the corresponding sample<sup>67</sup>. The read count was log2 transformed and quantile normalized across all samples. A modified t-test<sup>68</sup> and false discovery rate (FDR) analysis<sup>28</sup> were applied to identify differentially expressed miRNAs ( $p < 0.05$ ).

### miR-gene-GO enrichment analysis

miR-gene-GO enrichment analysis contains three steps [target prediction, target enrichment, and gene ontology (GO) term enrichment] as described previously<sup>27</sup>. In the first step, the target genes of differentially expressed miRNAs were predicted by using the target prediction tools TargetScan (<http://www.targetscan.org/>) and miRanda (<http://www.microrna.org/microrna/home.do>). Only target genes predicted by both TargetScan and miRanda were used in the next step of analysis. In the second step, the statistical significance of enrichment for each target gene identified in the first step was determined by using the hypergeometric test, and genes with a p-value  $< 10^{-5}$  were considered significantly enriched. In the last step, GO terms annotating enriched genes identified in the second step were obtained from the Gene Ontology database (<http://www.geneontology.org/>). As this database is constructed in the directed acyclic graph in which a parent GO term has multiple children terms, GO terms with redundant information are given to genes mapped to both parent and children terms. We therefore used the conditional hypergeometric test which removes the redundancy for the enrichment analysis. GO terms with a p-value  $< 0.05$  were considered significantly enriched.

Equation 1 was used for the hypergeometric statistical test in the gene enrichment analysis for each test group.

$$p - \text{value}_{\text{gene}} = \frac{\binom{n_{11} + n_{21}}{n_{11}} \binom{n_{12} + n_{22}}{n_{12}}}{\binom{n_{11} + n_{12} + n_{21} + n_{22}}{n_{11} + n_{12}}}, \text{ where } \begin{cases} \text{miRNAs in the test group} & n_{11} \\ \text{e. g. up-regulated miRNAs} & n_{12} \\ \text{target to the gene} & n_{21} \\ \text{not target to the gene} & n_{22} \end{cases}$$

$n_{11}$  = the number of miRNAs in the test group that target to the gene being tested;

$n_{12}$  = the number of other detected miRNAs that had the same change direction as those in the test group, and target to the gene being tested, but were not included in the test group because their FDR controlled p-values were greater than 0.05;

$n_{21}$  = the number of miRNAs in the group that do NOT target to the gene being tested;

$n_{22}$  = the number of other miRNAs that had the same change direction as those in the test group, but do NOT target to the gene being tested, and were not included in the test group because their FDR controlled p-values were greater than 0.05.

The enriched GO terms that annotate the over-represented genes were identified by using the conditional hypergeometric test (R package GOSTats). GO terms whose statistical significance was contributed by their significant children terms were removed in the

conditional hypergeometric test. GO terms that had p-values less than 0.05 and were targeted by at least 50% of the total selected miRNAs in the test group were considered statistically enriched. Equation 2 was used for the test. There were three sets of GO terms: biological process (BP), molecular function (MF), and cellular component (CC).

Conditional Hypergeometric test of a GO term annotating the over - represented genes

$$p - \text{value}_{GO - \text{term}} = \frac{\binom{m_{11}+m_{21}}{m_{11}} \binom{m_{12}+m_{22}}{m_{12}}}{\binom{m_{11}+m_{12}+m_{21}+m_{22}}{m_{11}+m_{12}}}, \text{ where } \left[ \begin{array}{l} \text{genes in the test group} \\ \text{other genes} \\ \text{mapped genes} \\ \text{not mapped genes} \end{array} \begin{array}{l} m_{11} \\ m_{12} \\ m_{21} \\ m_{22} \end{array} \right] \text{ Equa}$$

$m_{11}$  = the number of over-represented genes in the test group that were mapped to the GO term being tested;

$m_{12}$  = the number of other genes in the GO database that were mapped to the GO term being tested;

$m_{21}$  = the number of over-represented genes in the test group were NOT mapped to the GO term being tested;

$m_{22}$  = the number of other genes in the GO database that were NOT mapped to the GO term being tested.

### Quantitative reverse transcription PCR

miRNAs were purified by using the mirVana miRNA Isolation Kit (Ambion). miRNAs were transcribed into cDNAs and amplified by PCR with the Taqman primers (miR-106b, ID: 442; miR-135a, ID: 460; miR-135b, ID: 2261; miR-136-3p, ID: 2100; miR-19a, ID: 395; miR-19b, ID: 396; miR-191, ID: 2299; miR-466b, ID: 2066; miR-218, ID: 521; miR-29a, ID: 2112; miR-32, ID: 2109) specific for miRNAs of interest. Pri-miRNAs were purified using Trizol (Life technologies), transcribed into cDNAs and amplified by PCR with the primers as follows: miR-191, AGCTGCACTTGGATTTCGTT and TGGCCCAGTAGTGTCTCTGA; miR-135b, TTCCTGCTCTTTGAGATTCCT and GCTGGTCCTTAGGGAAGTGTA; U6, GCTTCGGCAGCACATATACTAA and AAAATATGGAACGCTTCACGA. Applied Biosystems 7900 Fast Real-Time PCR System was used for quantitative reverse transcription PCR. U6 (Taqman probe ID: 1973) was used as the endogenous control gene to normalize input amounts.

### Neuronal culture and transfection

Hippocampal and cortical neuron cultures were prepared from embryonic day (E) 18–19 rat embryos. The hippocampus was removed from the embryo brains, dissociated with trypsin and seeded on coverslips or plates coated with poly-D-lysine (30  $\mu\text{g}$  per ml) and laminin (2  $\mu\text{g}$  per ml) to a density of 750 cells per  $\text{mm}^2$  (for spine morphology analysis) or 450 cells per  $\text{mm}^2$  (for immunocytochemistry). Cultures were grown in Neurobasal medium supplemented with 2% B27, 2 mM glutamax. Hippocampal neurons were transfected with Lipofectamine 2000. All reagents for neuronal cultures were purchased from Invitrogen.

## Time-lapse imaging and FRAP

Cultured hippocampal neurons were placed in an imaging chamber and perfused with ACSF [composed of (in mM) 124 NaCl, 3 KCl, 26 NaHCO<sub>3</sub>, 1.25 NaH<sub>2</sub>PO<sub>4</sub>, 2.5 CaCl<sub>2</sub>, 1.3 MgSO<sub>4</sub>, and 10 D-glucose; bubbled with 95% O<sub>2</sub>/5% CO<sub>2</sub>; 30°C] at 2 ml/min. Images were acquired by using an Olympus BX61WI confocal microscope with a 60X objective (NA 1.35). Z-stack images were collapsed to make 2D projections for image analysis. Spine area and density were analyzed by using MetaMorph software (Molecular Devices). Briefly, images were thresholded to remove background. Spines in secondary dendrites were then manually selected and analyzed for area and number by using the 'Integrated Morphometry Analysis' function of MetaMorph. The length of dendrites was measured by using the 'Region measurement' function of MetaMorph. Spine density was calculated by dividing the total number of spines on a given dendrite by the length of the dendrite.

Photobleaching of dendrites was performed using the photobleach function of the Olympus Fluoview software. The region of interest was scanned with 100% laser intensity for 30 s followed by normal imaging mode. The integrated SEP intensity of photobleached dendrites at each time point was measured using MetaMorph software, and normalized to that of unbleached dendrites to correct for possible fluorescence decay due to repetitive image acquisition. The proportion of recovered SEP at each time point after bleaching (corrected fluorescence intensity/pre-bleaching fluorescence intensity) was fitted to an exponential curve using the equation  $F(t) = F - Ae^{-t/\tau}$ , where  $F(t)$  is fluorescence at time  $t$ ,  $F$  is the steady state fluorescence after recovery,  $A$  is the residual fluorescence after photobleaching, and  $\tau$  is time constant. The image data were analyzed with the Kolmogorov-Smirnov and Chi-Squared test for distribution. As the image data are not normally distributed, two-tailed Mann-Whitney U test was used to calculate p-values.

## Immunocytochemistry

Hippocampal neurons were fixed in PBS containing 4% formaldehyde and 4% sucrose. After rinse, neurons were incubated with primary antibodies overnight at 4°C, followed by incubation with fluorophore-conjugated secondary antibodies. Z stack Images were acquired by using a Zeiss LSM510 confocal microscope with a 63x (NA 1.4) or 40x (NA 1.2) objective, and collapsed to make 2D projections. MetaMorph software (Molecular Devices) was used to measure integrated fluorescence intensity of Phalloidin, Tmod2, and Complexin 1/2 on the dendrite. All image acquisition and image analysis were done blindly to treatment. The image data were analyzed with the Kolmogorov-Smirnov and Chi-Squared test for distribution. As the image data are not normally distributed, two-tailed Mann-Whitney U test was used to calculate p-values.

## Hippocampal slice culture

Hippocampal slices were cultured from 6- to 8-day-old Sprague-Dawley rats. After decapitation, the brain was placed immediately in the cold cutting solution (238 mM sucrose, 2.5 mM KCl, 26 mM NaHCO<sub>3</sub>, 1 mM NaH<sub>2</sub>PO<sub>4</sub>, 5 mM MgCl<sub>2</sub>, 11 mM D-glucose, and 1 mM CaCl<sub>2</sub>). Hippocampal slices (400  $\mu$ m) were cut with a vibratome (Leica) and placed on top of semipermeable membrane inserts (Millipore Corporation) in a 6-well plate containing culture medium (78.8% minimum essential medium, 20% heat-inactivated horse

serum, 25 mM HEPES, 10 mM D-glucose, 26 mM NaHCO<sub>3</sub>, 2 mM CaCl<sub>2</sub>, 2 mM MgSO<sub>4</sub>, 0.0012% ascorbic acid, 1 μg ml<sup>-1</sup> insulin; pH 7.3; 320–330 mOsm). Medium was changed every 2 days. No antibiotics were used. Slices were transduced with lentivirus at DIV12 and used for electrophysiology at DIV17.

### Electrophysiology

Hippocampal slices were perfused with artificial cerebrospinal fluid (ACSF, pH 7.4, gassed with 95% O<sub>2</sub>/5% CO<sub>2</sub>, composed of in mM: 124 NaCl, 3 KCl, 26 NaHCO<sub>3</sub>, 1.25 NaH<sub>2</sub>PO<sub>4</sub>, 2.5 CaCl<sub>2</sub>, 1.3 MgSO<sub>4</sub>, and 10 D-glucose bubbled with 95% O<sub>2</sub> / 5% CO<sub>2</sub>; 30°C) at the rate of 2 ml/min. The stimulating electrode was placed on the stratum radiatum in the CA2 area. Stimuli were delivered to the electrode at 20 sec intervals. Recording pipettes (1–2 MΩ) were filled with the bath solution and placed in the CA1 region. The stimulating electrode was placed at the stratum radiatum in the CA2 area. A 30 min-baseline recording was conducted prior to LTD induction. LTD was induced by delivering low-frequency stimulations (900 pulses at 1 Hz). The electrophysiology data were analyzed with the Kolmogorov-Smirnov and Chi-Squared test for distribution. As the electrophysiology data are not normally distributed, two-tailed Mann-Whitney U test was used to calculate p-values.

### *In situ* hybridization

*In situ* hybridization of microRNA was performed as described<sup>69</sup>. Briefly, Hippocampal neurons were fixed in PBS containing 4% formaldehyde and 4% sucrose. After permeabilization with PBS/0.5% Triton X-100, neurons were hybridized with 5' and 3' digoxigenin-labeled, locked nucleic acid (LNA)-modified oligonucleotide probes (Exiqon) for detection of miRNAs or in vitro transcribed, digoxigenin-labeled RNAs for detection of mRNAs. Hybridized probes were detected by incubation with horseradish peroxidase-conjugated anti-digoxigenin antibody (Roche) followed by amplification with Cy5-conjugated tyramide (Perkin Elmer).

### Cross-linking and immunoprecipitation assay

Cultured cortical neurons grown on 10 cm dishes were transduced with lentivirus expressing Flag-tagged Ago2 at DIV 7, and treated with NMDA at DIV 17. Cross-linking and immunoprecipitation of Ago2-associated RNA was performed as described with modifications<sup>70</sup>. At 90min after NMDA treatment, neurons were crosslinked with UV irradiation (480,000 μJ cm<sup>-2</sup>), and then lysed in 1XRIPA buffer containing 0.1 U μL<sup>-1</sup> RNase inhibitor followed by sonication. After centrifugation at 13,000 rpm for 30 min at 4°C, supernatant was incubated with anti-Flag antibody-conjugated beads (Sigma-aldrich) overnight with rotation at 4°C. The beads were washed 5 times with immunoprecipitation buffer [25mM HEPES (PH7.5), 150mM NaCl, 0.5mM EDTA, 1mM EGTA, 10% Glycerol, 0.1% NP40, 1mM NaF, 1mM 2-glycerophosphate, 1mM Na<sub>3</sub>VO<sub>4</sub>]. Bound RNAs were extracted with phenol/chloroform, precipitated with ethanol, and analyzed by qRT-PCR.

### Supplementary Material

Refer to Web version on PubMed Central for supplementary material.

## Acknowledgements

We thank Dr. Song Jiao for help with preparation of acute hippocampal slices, Dr. Heinz Arnheiter for intense discussions of this study and critical reading of the manuscript and Dr. Elizabeth J. Sherman for a close reading and editing of the manuscript. This work was supported by the NIMH and the NHLBI Intramural Programs.

## References

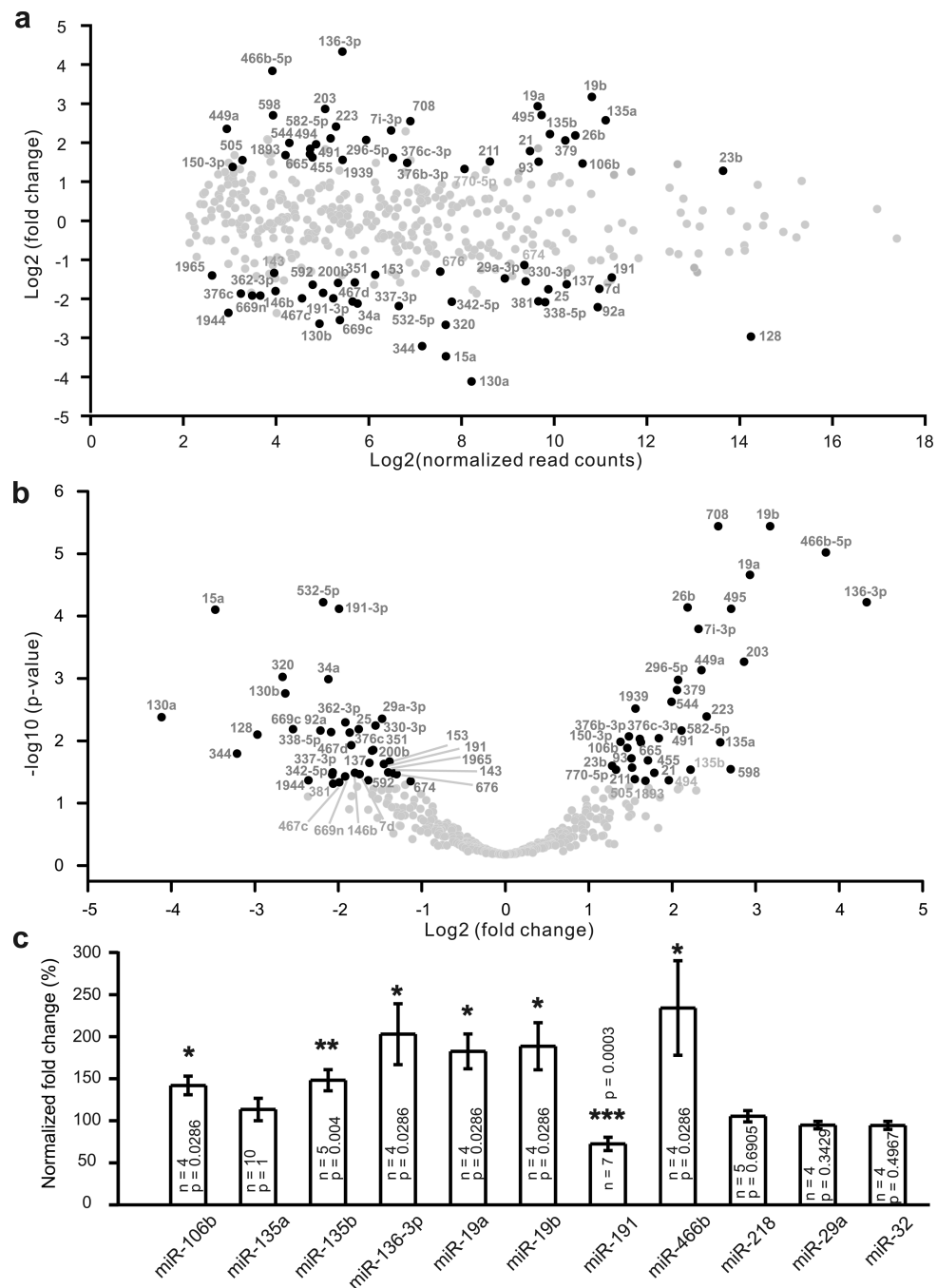
1. Bhatt DH, Zhang S, Gan WB. Dendritic spine dynamics. *Annu Rev Physiol.* 2009; 71:261–282. [PubMed: 19575680]
2. Asrican B, Lisman J, Otmakhov N. Synaptic strength of individual spines correlates with bound Ca<sup>2+</sup>-calmodulin-dependent kinase II. *J Neurosci.* 2007; 27:14007–14011. [PubMed: 18094239]
3. Matsuzaki M, et al. Dendritic spine geometry is critical for AMPA receptor expression in hippocampal CA1 pyramidal neurons. *Nat Neurosci.* 2001; 4:1086–1092. [PubMed: 11687814]
4. Segal M. Dendritic spines and long-term plasticity. *Nat Rev Neurosci.* 2005; 6:277–284. [PubMed: 15803159]
5. Zhou Q, Homma KJ, Poo MM. Shrinkage of dendritic spines associated with long-term depression of hippocampal synapses. *Neuron.* 2004; 44:749–757. [PubMed: 15572107]
6. Nagerl UV, Eberhorn N, Cambridge SB, Bonhoeffer T. Bidirectional activity-dependent morphological plasticity in hippocampal neurons. *Neuron.* 2004; 44:759–767. [PubMed: 15572108]
7. Fu M, Yu X, Lu J, Zuo Y. Repetitive motor learning induces coordinated formation of clustered dendritic spines in vivo. *Nature.* 2012; 483:92–95. [PubMed: 22343892]
8. Hofer SB, Mrsic-Flogel TD, Bonhoeffer T, Hubener M. Experience leaves a lasting structural trace in cortical circuits. *Nature.* 2009; 457:313–317. [PubMed: 19005470]
9. Brigman JL, et al. Loss of GluN2B-containing NMDA receptors in CA1 hippocampus and cortex impairs long-term depression, reduces dendritic spine density, and disrupts learning. *J Neurosci.* 2010; 30:4590–4600. [PubMed: 20357110]
10. Nicholls RE, et al. Transgenic mice lacking NMDAR-dependent LTD exhibit deficits in behavioral flexibility. *Neuron.* 2008; 58:104–117. [PubMed: 18400167]
11. Wong TP, et al. Hippocampal long-term depression mediates acute stress-induced spatial memory retrieval impairment. *Proc Natl Acad Sci U S A.* 2007; 104:11471–11476. [PubMed: 17592137]
12. Wang XB, Yang Y, Zhou Q. Independent expression of synaptic and morphological plasticity associated with long-term depression. *J Neurosci.* 2007; 27:12419–12429. [PubMed: 17989307]
13. He K, Lee A, Song L, Kanold PO, Lee HK. AMPA receptor subunit GluR1 (GluA1) serine-845 site is involved in synaptic depression but not in spine shrinkage associated with chemical long-term depression. *J Neurophysiol.* 2011; 105:1897–1907. [PubMed: 21307330]
14. Fabian MR, Sonenberg N, Filipowicz W. Regulation of mRNA translation and stability by microRNAs. *Annu Rev Biochem.* 2010; 79:351–379. [PubMed: 20533884]
15. Bartel DP. MicroRNAs: genomics, biogenesis, mechanism, and function. *Cell.* 2004; 116:281–297. [PubMed: 14744438]
16. Siegel G, Saba R, Schrott G. microRNAs in neurons: manifold regulatory roles at the synapse. *Curr Opin Genet Dev.* 2011; 21:491–497. [PubMed: 21561760]
17. Ling KH, et al. Deep sequencing analysis of the developing mouse brain reveals a novel microRNA. *BMC Genomics.* 2011; 12:176. [PubMed: 21466694]
18. Shao NY, et al. Comprehensive survey of human brain microRNA by deep sequencing. *BMC Genomics.* 2010; 11:409. [PubMed: 20591156]
19. Fenelon K, et al. Deficiency of Dgcr8, a gene disrupted by the 22q11.2 microdeletion, results in altered short-term plasticity in the prefrontal cortex. *Proc Natl Acad Sci U S A.* 2011; 108:4447–4452. [PubMed: 21368174]
20. Konopka W, et al. MicroRNA loss enhances learning and memory in mice. *J Neurosci.* 2010; 30:14835–14842. [PubMed: 21048142]

21. Lee K, et al. An activity-regulated microRNA, miR-188, controls dendritic plasticity and synaptic transmission by downregulating neuropilin-2. *J Neurosci.* 2012; 32:5678–5687. [PubMed: 22514329]
22. Lippi G, et al. Targeting of the Arpc3 actin nucleation factor by miR-29a/b regulates dendritic spine morphology. *J Cell Biol.* 2011; 194:889–904. [PubMed: 21930776]
23. Park CS, Tang SJ. Regulation of microRNA expression by induction of bidirectional synaptic plasticity. *J Mol Neurosci.* 2009; 38:50–56. [PubMed: 18998061]
24. Huang YW, Ruiz CR, Eyler EC, Lin K, Meffert MK. Dual regulation of miRNA biogenesis generates target specificity in neurotrophin-induced protein synthesis. *Cell.* 2012; 148:933–946. [PubMed: 22385959]
25. Lee HK, Kameyama K, Hugarir RL, Bear MF. NMDA induces long-term synaptic depression and dephosphorylation of the GluR1 subunit of AMPA receptors in hippocampus. *Neuron.* 1998; 21:1151–1162. [PubMed: 9856470]
26. Beattie EC, et al. Regulation of AMPA receptor endocytosis by a signaling mechanism shared with LTD. *Nat Neurosci.* 2000; 3:1291–1300. [PubMed: 11100150]
27. Hu Z, et al. Expression of miRNAs and their cooperative regulation of the pathophysiology in traumatic brain injury. *PLoS One.* 2012; 7:e39357. [PubMed: 22761770]
28. Strimmer K. fdrtool: a versatile R package for estimating local and tail area-based false discovery rates. *Bioinformatics.* 2008; 24:1461–1462. [PubMed: 18441000]
29. Fischer RS, Fowler VM. Tropomodulins: life at the slow end. *Trends Cell Biol.* 2003; 13:593–601. [PubMed: 14573353]
30. Ahmad M, et al. Postsynaptic complexin controls AMPA receptor exocytosis during LTP. *Neuron.* 2012; 73:260–267. [PubMed: 22284181]
31. Bosch M, Hayashi Y. Structural plasticity of dendritic spines. *Curr Opin Neurobiol.* 2012; 22:383–388. [PubMed: 21963169]
32. Thomas GM, Hugarir RL. MAPK cascade signalling and synaptic plasticity. *Nat Rev Neurosci.* 2004; 5:173–183. [PubMed: 14976517]
33. Nagai T, et al. A variant of yellow fluorescent protein with fast and efficient maturation for cell-biological applications. *Nat Biotechnol.* 2002; 20:87–90. [PubMed: 11753368]
34. Garcia DM, et al. Weak seed-pairing stability and high target-site abundance decrease the proficiency of lsy-6 and other microRNAs. *Nat Struct Mol Biol.* 2011; 18:1139–1146. [PubMed: 21909094]
35. Lewis BP, Burge CB, Bartel DP. Conserved seed pairing, often flanked by adenosines, indicates that thousands of human genes are microRNA targets. *Cell.* 2005; 120:15–20. [PubMed: 15652477]
36. Di Leva G, et al. Estrogen mediated-activation of miR-191/425 cluster modulates tumorigenicity of breast cancer cells depending on estrogen receptor status. *PLoS Genet.* 2013; 9:e1003311. [PubMed: 23505378]
37. Watakabe A, Kobayashi R, Helfman DM. N-tropomodulin: a novel isoform of tropomodulin identified as the major binding protein to brain tropomyosin. *J Cell Sci.* 1996; 109(Pt 9):2299–2310. [PubMed: 8886980]
38. Brose N. For better or for worse: complexins regulate SNARE function and vesicle fusion. *Traffic.* 2008; 9:1403–1413. [PubMed: 18445121]
39. Sudhof TC, Rothman JE. Membrane fusion: grappling with SNARE and SM proteins. *Science.* 2009; 323:474–477. [PubMed: 19164740]
40. Park M, et al. Plasticity-induced growth of dendritic spines by exocytic trafficking from recycling endosomes. *Neuron.* 2006; 52:817–830. [PubMed: 17145503]
41. Makino H, Malinow R. AMPA receptor incorporation into synapses during LTP: the role of lateral movement and exocytosis. *Neuron.* 2009; 64:381–390. [PubMed: 19914186]
42. Ashby MC, et al. Removal of AMPA receptors (AMPA receptors) from synapses is preceded by transient endocytosis of extrasynaptic AMPARs. *J Neurosci.* 2004; 24:5172–5176. [PubMed: 15175386]

43. Sharma K, Fong DK, Craig AM. Postsynaptic protein mobility in dendritic spines: long-term regulation by synaptic NMDA receptor activation. *Mol Cell Neurosci.* 2006; 31:702–712. [PubMed: 16504537]
44. Siegel G, et al. A functional screen implicates microRNA-138-dependent regulation of the depalmitoylation enzyme APT1 in dendritic spine morphogenesis. *Nat Cell Biol.* 2009; 11:705–716. [PubMed: 19465924]
45. Traynelis SF, et al. Glutamate receptor ion channels: structure, regulation, and function. *Pharmacol Rev.* 2010; 62:405–496. [PubMed: 20716669]
46. Kye MJ, et al. NMDA mediated contextual conditioning changes miRNA expression. *PLoS One.* 2011; 6:e24682. [PubMed: 21931811]
47. Wibrand K, et al. Differential regulation of mature and precursor microRNA expression by NMDA and metabotropic glutamate receptor activation during LTP in the adult dentate gyrus in vivo. *Eur J Neurosci.* 2010; 31:636–645. [PubMed: 20384810]
48. Kauderer BS, Kandel ER. Capture of a protein synthesis-dependent component of long-term depression. *Proc Natl Acad Sci U S A.* 2000; 97:13342–13347. [PubMed: 11087874]
49. Manahan-Vaughan D, Kulla A, Frey JU. Requirement of translation but not transcription for the maintenance of long-term depression in the CA1 region of freely moving rats. *J Neurosci.* 2000; 20:8572–8576. [PubMed: 11069965]
50. Sajikumar S, Frey JU. Anisomycin inhibits the late maintenance of long-term depression in rat hippocampal slices in vitro. *Neurosci Lett.* 2003; 338:147–150. [PubMed: 12566174]
51. Okamoto K, Nagai T, Miyawaki A, Hayashi Y. Rapid and persistent modulation of actin dynamics regulates postsynaptic reorganization underlying bidirectional plasticity. *Nat Neurosci.* 2004; 7:1104–1112. [PubMed: 15361876]
52. Nakamura Y, et al. PICK1 inhibition of the Arp2/3 complex controls dendritic spine size and synaptic plasticity. *EMBO J.* 2011; 30:719–730. [PubMed: 21252856]
53. Pontrello CG, et al. Cofilin under control of beta-arrestin-2 in NMDA-dependent dendritic spine plasticity, long-term depression (LTD), and learning. *Proc Natl Acad Sci U S A.* 2012; 109:E442–E451. [PubMed: 22308427]
54. Collingridge GL, Isaac JT, Wang YT. Receptor trafficking and synaptic plasticity. *Nat Rev Neurosci.* 2004; 5:952–962. [PubMed: 15550950]
55. Shepherd JD, Huganir RL. The cell biology of synaptic plasticity: AMPA receptor trafficking. *Annu Rev Cell Dev Biol.* 2007; 23:613–643. [PubMed: 17506699]
56. Malenka RC, Bear MF. LTP and LTD: an embarrassment of riches. *Neuron.* 2004; 44:5–21. [PubMed: 15450156]
57. Patterson MA, Szatmari EM, Yasuda R. AMPA receptors are exocytosed in stimulated spines and adjacent dendrites in a Ras-ERK-dependent manner during long-term potentiation. *Proc Natl Acad Sci U S A.* 2010; 107:15951–15956. [PubMed: 20733080]
58. Hayashi Y, et al. Driving AMPA receptors into synapses by LTP and CaMKII: requirement for GluR1 and PDZ domain interaction. *Science.* 2000; 287:2262–2267. [PubMed: 10731148]
59. Park M, Penick EC, Edwards JG, Kauer JA, Ehlers MD. Recycling endosomes supply AMPA receptors for LTP. *Science.* 2004; 305:1972–1975. [PubMed: 15448273]
60. Lu W, et al. Activation of synaptic NMDA receptors induces membrane insertion of new AMPA receptors and LTP in cultured hippocampal neurons. *Neuron.* 2001; 29:243–254. [PubMed: 11182095]
61. Bicker S, et al. The DEAH-box helicase DHX36 mediates dendritic localization of the neuronal precursor-microRNA-134. *Genes Dev.* 2013; 27:991–996. [PubMed: 23651854]
62. Maghsoodi B, et al. Retinoic acid regulates RARalpha-mediated control of translation in dendritic RNA granules during homeostatic synaptic plasticity. *Proc Natl Acad Sci U S A.* 2008; 105:16015–16020. [PubMed: 18840692]
63. Sutton MA, et al. Miniature neurotransmission stabilizes synaptic function via tonic suppression of local dendritic protein synthesis. *Cell.* 2006; 125:785–799. [PubMed: 16713568]
64. Richter JD, Klann E. Making synaptic plasticity and memory last: mechanisms of translational regulation. *Genes Dev.* 2009; 23:1–11. [PubMed: 19136621]

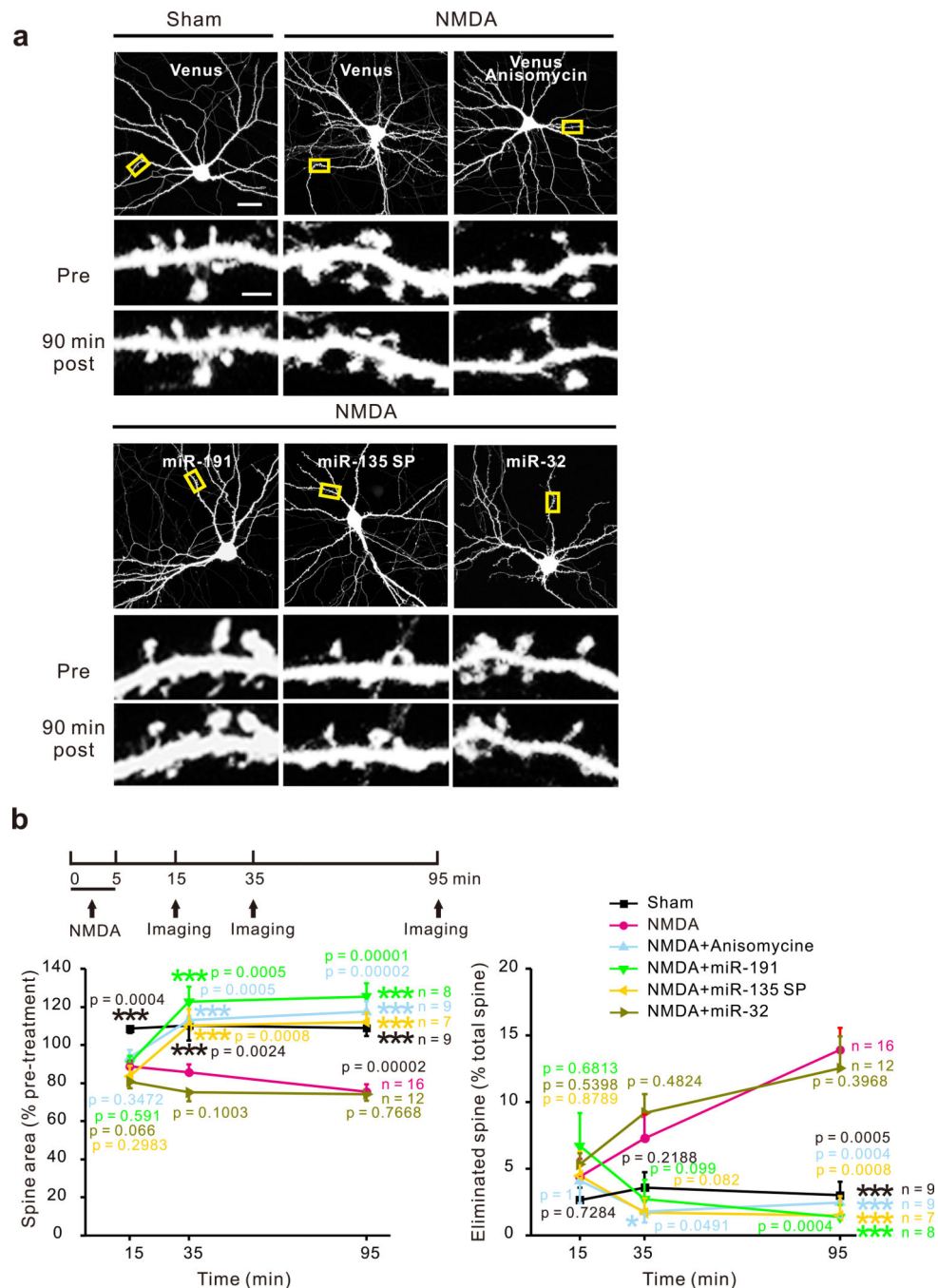
65. Ebert MS, Neilson JR, Sharp PA. MicroRNA sponges: competitive inhibitors of small RNAs in mammalian cells. *Nat Methods*. 2007; 4:721–726. [PubMed: 17694064]
66. Langmead B, Trapnell C, Pop M, Salzberg SL. Ultrafast and memory-efficient alignment of short DNA sequences to the human genome. *Genome Biol*. 2009; 10:R25. [PubMed: 19261174]
67. Bolstad BM, Irizarry RA, Astrand M, Speed TP. A comparison of normalization methods for high density oligonucleotide array data based on variance and bias. *Bioinformatics*. 2003; 19:185–193. [PubMed: 12538238]
68. Smyth GK. Linear models and empirical bayes methods for assessing differential expression in microarray experiments. *Stat Appl Genet Mol Biol*. 2004; 3 Article3.
69. de Planell-Saguer M, Rodicio MC, Mourelatos Z. Rapid in situ codetection of noncoding RNAs and proteins in cells and formalin-fixed paraffin-embedded tissue sections without protease treatment. *Nat Protoc*. 2010; 5:1061–1073. [PubMed: 20539282]
70. Kang JG, et al. Kaposi's sarcoma-associated herpesvirus ORF57 promotes escape of viral and human interleukin-6 from microRNA-mediated suppression. *J Virol*. 2011; 85:2620–2630. [PubMed: 21209110]



**Figure 1.**

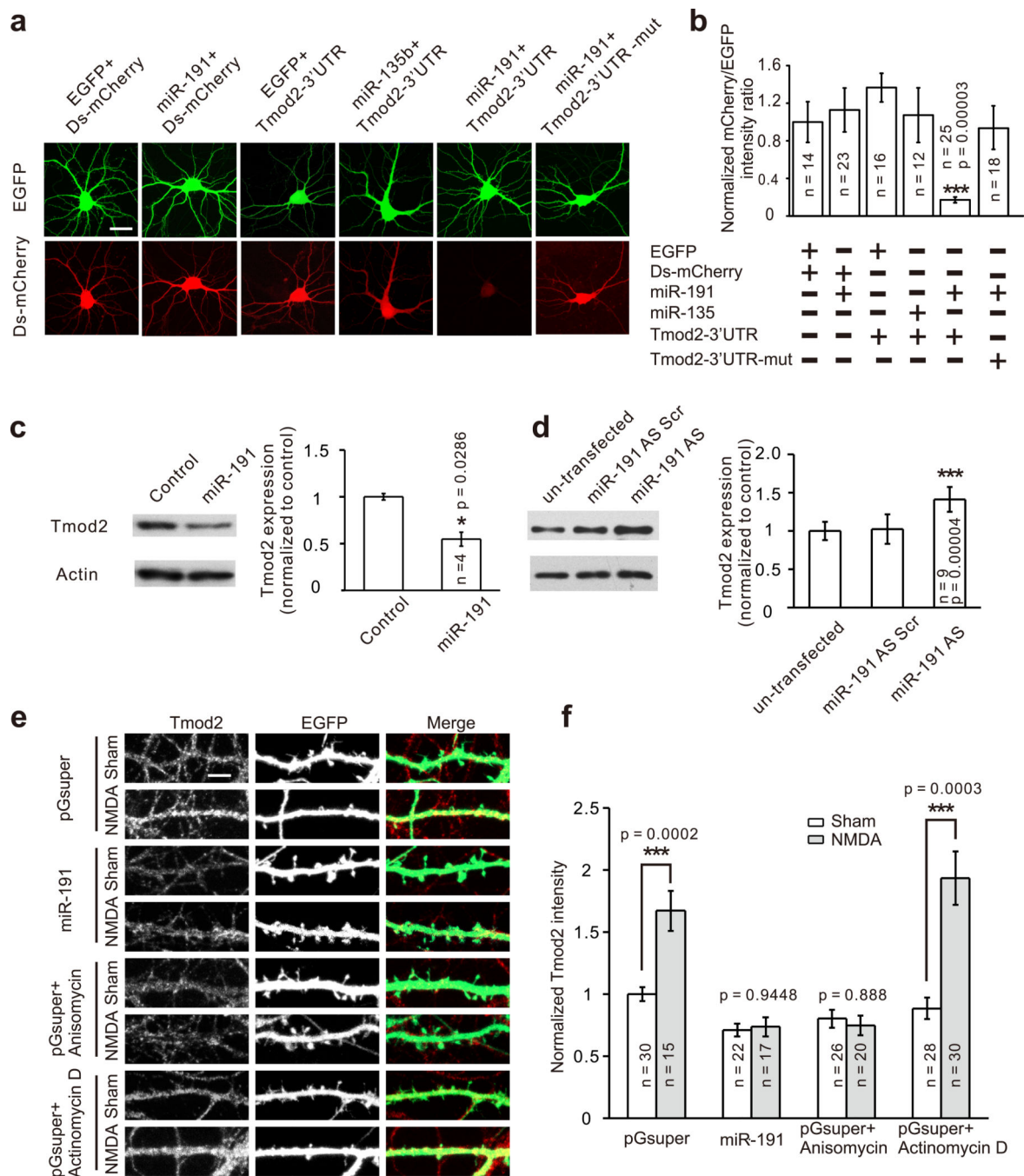
The change of miRNA transcriptomes in the hippocampus following LTD induction. Hippocampal slices were prepared from mice (17–19 days old) and either sham treated or treated with NMDA (30 $\mu$ M, 5 min) to induce chemical LTD. miRNAs were isolated at 90 min after NMDA treatment for deep sequencing (a, b) or qRT-PCR (c). (a) The fold change (log<sub>2</sub> scale) of each miRNA species is plotted against its normalized read number (log<sub>2</sub> scale). (b) The p-value (log<sub>10</sub> scale) of each miRNA species is plotted against its fold change (log<sub>2</sub> scale). (c) qRT-PCR analysis of miRNA expression. n = 4–10 experiments for

each miRNA. In a and b, miRNAs with p-values less than 0.05 are represented by dark circles. In c, data are presented as mean  $\pm$  SEM; Mann-Whitney U test is used for statistical analysis; \* p < 0.05, \*\* p < 0.01, \*\*\* p < 0.005.



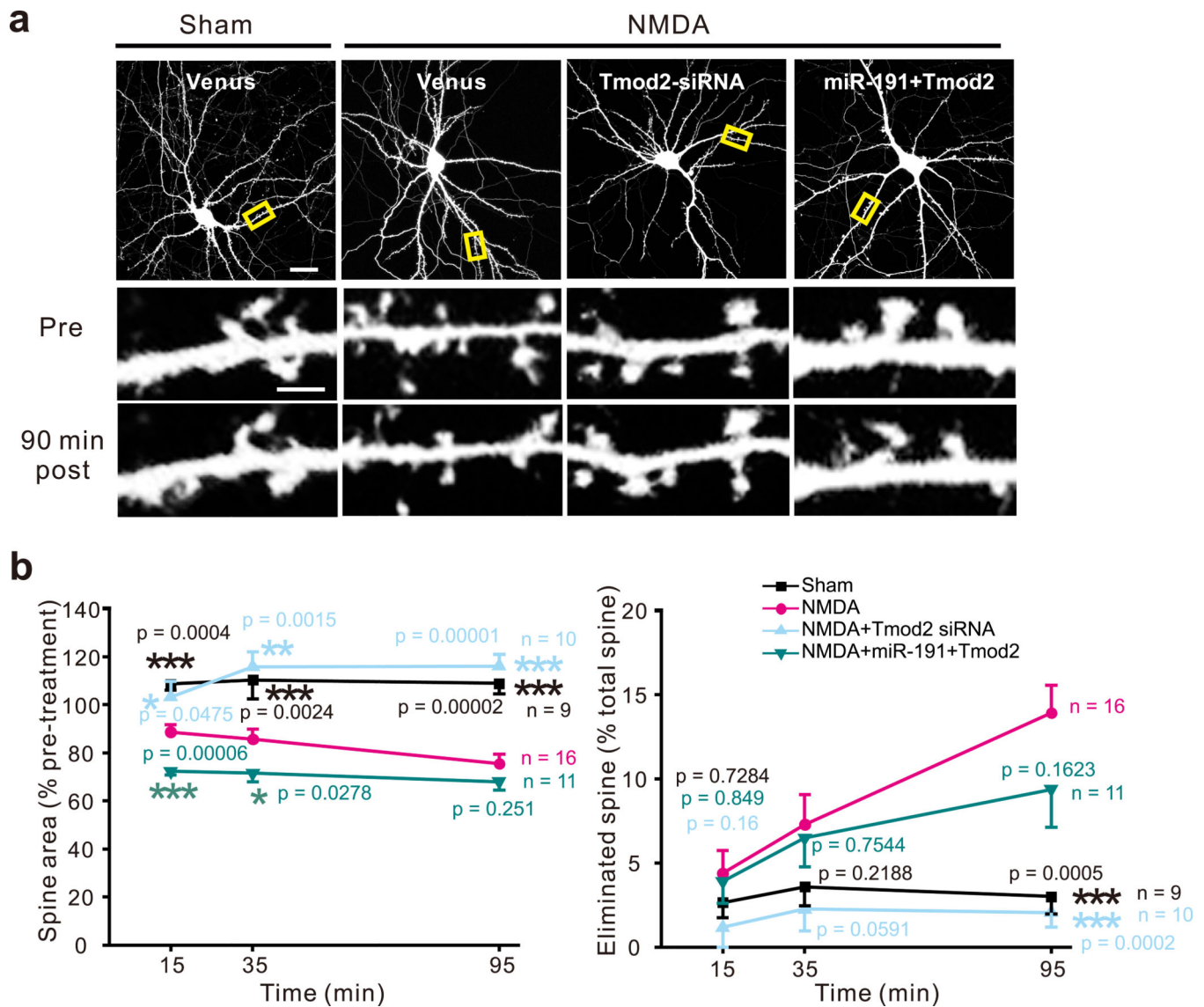
**Figure 2.** miR-191 and miR-135 are essential for long-lasting spine restructuring accompanying LTD. Cultured hippocampal neurons (DIV14) were transfected with the venus construct alone or along with the construct expressing miR-191, miR-32 or sponge against miR-135a and miR-135b. At 3–5 days after transfection, neurons were imaged before and at 10, 30 and 90 min after treatment. Anisomycin (20  $\mu$ M) was added to the bath solution at 10 min before NMDA treatment (30  $\mu$ M, 5 min) and present throughout the imaging period. (a) Representative images. Yellow boxes indicate the dendrites in the high magnification

images. (b) Quantification of a.  $n = 7-16$  neurons for each group. Data are presented as mean  $\pm$  SEM. Mann-Whitney U test was used for statistical analysis of the NMDA treated, venus transfected group vs. other groups. \*\*\*  $p < 0.005$ . Scale bars, 20  $\mu\text{m}$  in the top image of a, 5  $\mu\text{m}$  in the high magnification image of a.

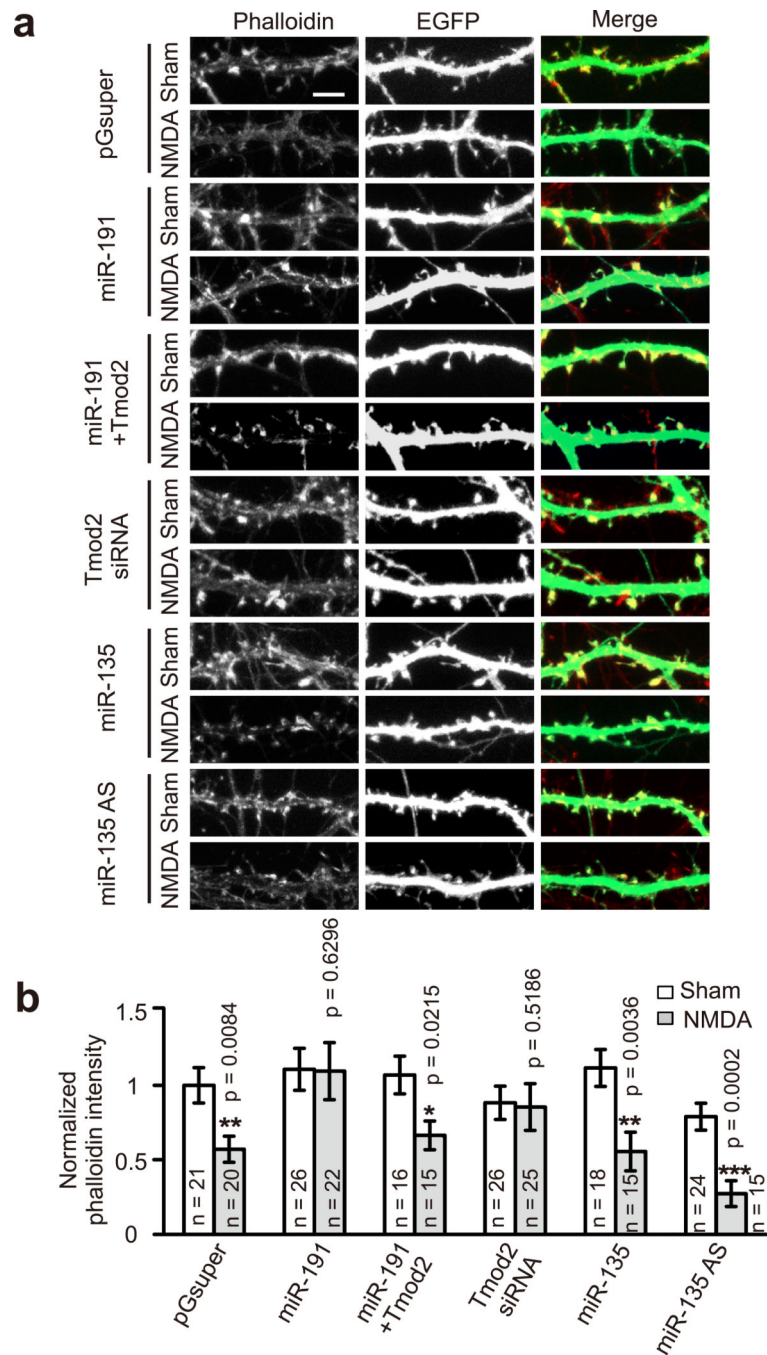
**Figure 3.**

Tmod2 is a physiological target of miR-191 and increased in expression by NMDA treatment. Cultured hippocampal neurons (a, b, e, f) and cortical neurons (c, d) were transfected with designated constructs at DIV14 or transduced with lentivirus at DIV7, and imaged or harvested for immunoblotting at DIV17. (a) Representative images of neurons co-transfected with the miRNA and reporter constructs. (b) Quantification of a. (c) Western blots of cell lysates from neurons transduced with the miR-191 or control virus; n = 4 experiments. (d) Western blots of cell lysates from neurons transfected with the miR-191

antisense oligonucleotides or scrambled oligonucleotides; n = 4–9 experiments for each condition. (e) Representative images of dendrites transfected with the miR-191 construct or the control plasmid. (f) Quantification of e. n = 12–30 cells for each group in b and f. Data are presented as mean  $\pm$  SEM. Mann-Whitney U test was used for statistical analysis. \*\*\* p < 0.005. Scale bars, 20  $\mu$ m in a, 5  $\mu$ m in e.



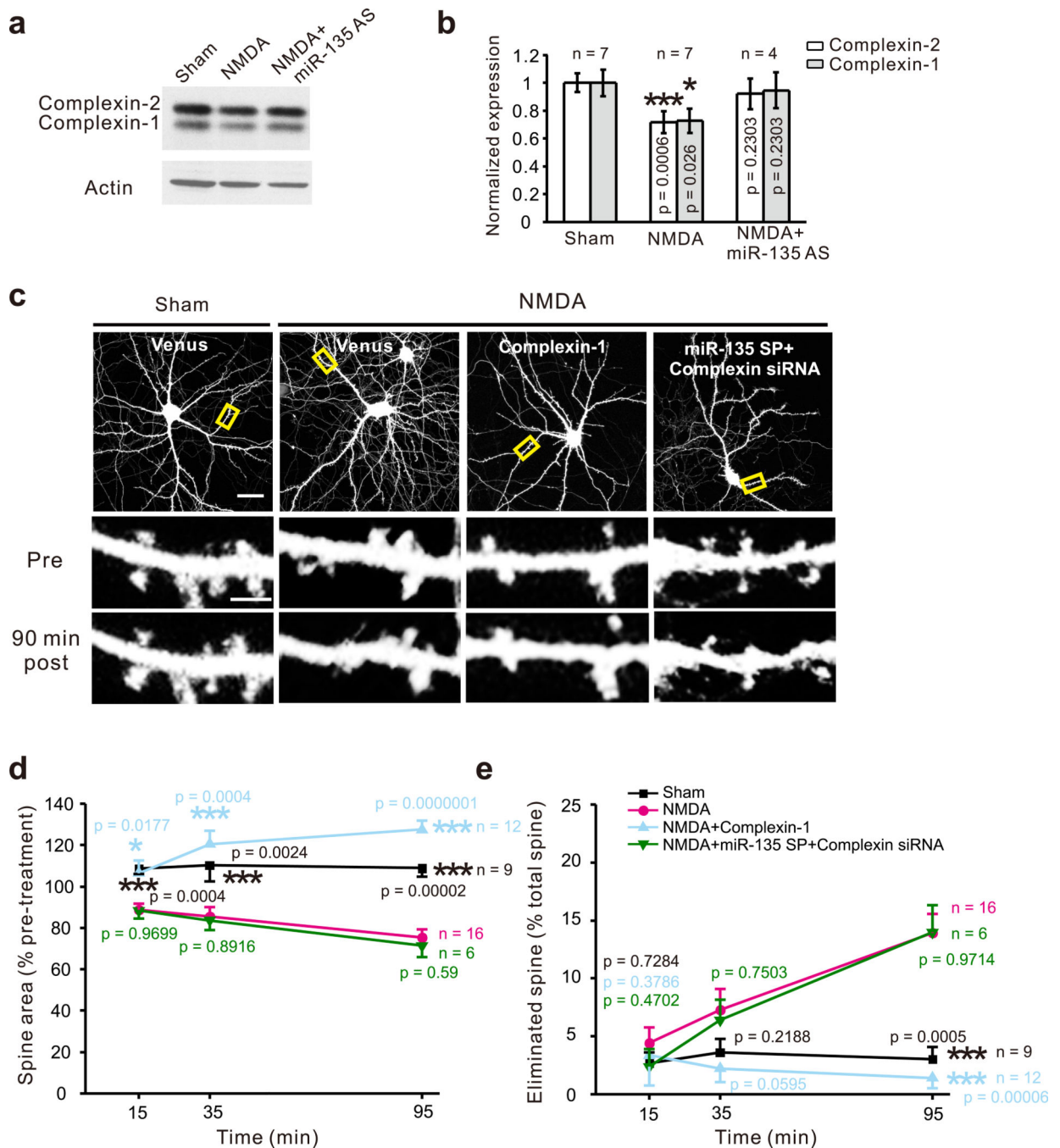
**Figure 4.** Tmod2 mediates the effect of miR-191 on spine remodeling during LTD. Cultured hippocampal neurons (DIV14) were transfected with the venus construct alone or along with the designated constructs. At 3–5 days after transfection, neurons were imaged before and at 10, 30 and 90 min after treatment. (a) Representative images. Yellow boxes indicate the dendrites in the high magnification images. (b) Quantification of a.  $n = 8$ –16 neurons for each group. Data are presented as mean  $\pm$  SEM. Mann-Whitney U test was used for statistical analysis of the NMDA treated, venus transfected group vs. other groups. \*  $p < 0.05$ , \*\*  $p < 0.01$ , \*\*\*  $p < 0.005$ . Scale bars, 20  $\mu\text{m}$  in the top image, 5  $\mu\text{m}$  in the high magnification image.



**Figure 5.**

Tmod2 is required for NMDA-induced reduction in actin filament. Cultured hippocampal neurons (DIV14) were transfected with the designated constructs. At DIV17, neurons were stained with rhodamine phalloidin at 90 min after NMDA treatment (30  $\mu$ M, 5 min). (a) Representative images of transfected dendrites. (b) Integrated fluorescence intensity of phalloidin/ $\mu$ m<sup>2</sup> dendrite area normalized to the sham treated group. n=15–26 neurons for each group. Data are presented as mean  $\pm$  SEM. Mann-Whitney U test was used for statistical analysis. \* p < 0.05, \*\* p < 0.01, \*\*\* p < 0.005. Scale bar, 5  $\mu$ m.



**Figure 6.**

Complexins mediate the effect of miR-135 on spine remodeling during LTD. Cultured cortical neurons (DIV14) were transfected with antisense oligonucleotides against miR-135 and treated with NMDA, followed by immunoblotting against complexin-1 and -2 in a and b. In c-e, cultured hippocampal neurons (DIV14) were transfected with the venus construct alone or along with the designated construct. At 3–5 days after transfection, neurons were imaged before and at 10, 30, and 90 min after treatment. (a) Representative blots. (b) Quantification of a. n = 4–7 experiments for each condition. (c) Representative images.

Yellow boxes indicate the dendrites in the high magnification images. (d, e) Quantification of c. n = 6–16 neurons for each group in d and e. Data are presented as mean  $\pm$  SEM. Mann-Whitney U test was used for statistical analysis of the NMDA treated, venus transfected group vs. other groups. \* p < 0.05, \*\* p < 0.01, \*\*\* p < 0.005. Scale bars, 20  $\mu$ m in the top image of c, 5  $\mu$ m in the high magnification image of c.

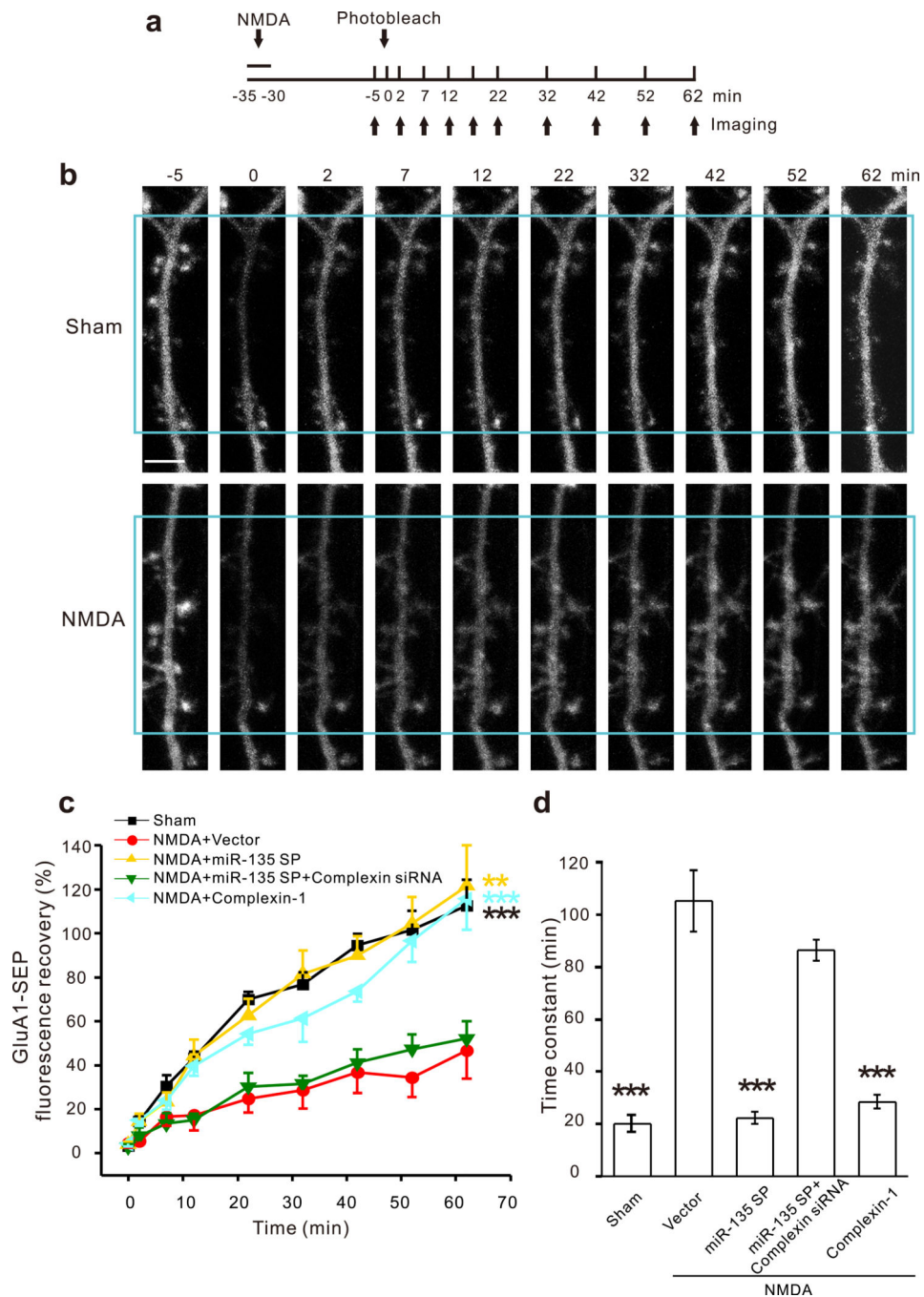


**Figure 7.** Inhibition of GluA1 exocytosis by miR-135 following NMDA treatment. Cultured hippocampal neurons (DIV14) were transfected with the DsRed and GluA1-SEP constructs, along with the designated plasmids. At 3–5 days after transfection, neurons were treated with NMDA (30  $\mu$ M, 5 min), photobleached and imaged at various time points as indicated. (a) Schematic drawing of the experimental design. (b) Representative images. Dendritic regions in the blue boxes were photobleached. (c) Fluorescence recovery curve of each group. (d) Time constant of fluorescence recovery after photobleaching.  $n = 5$ –12 neurons

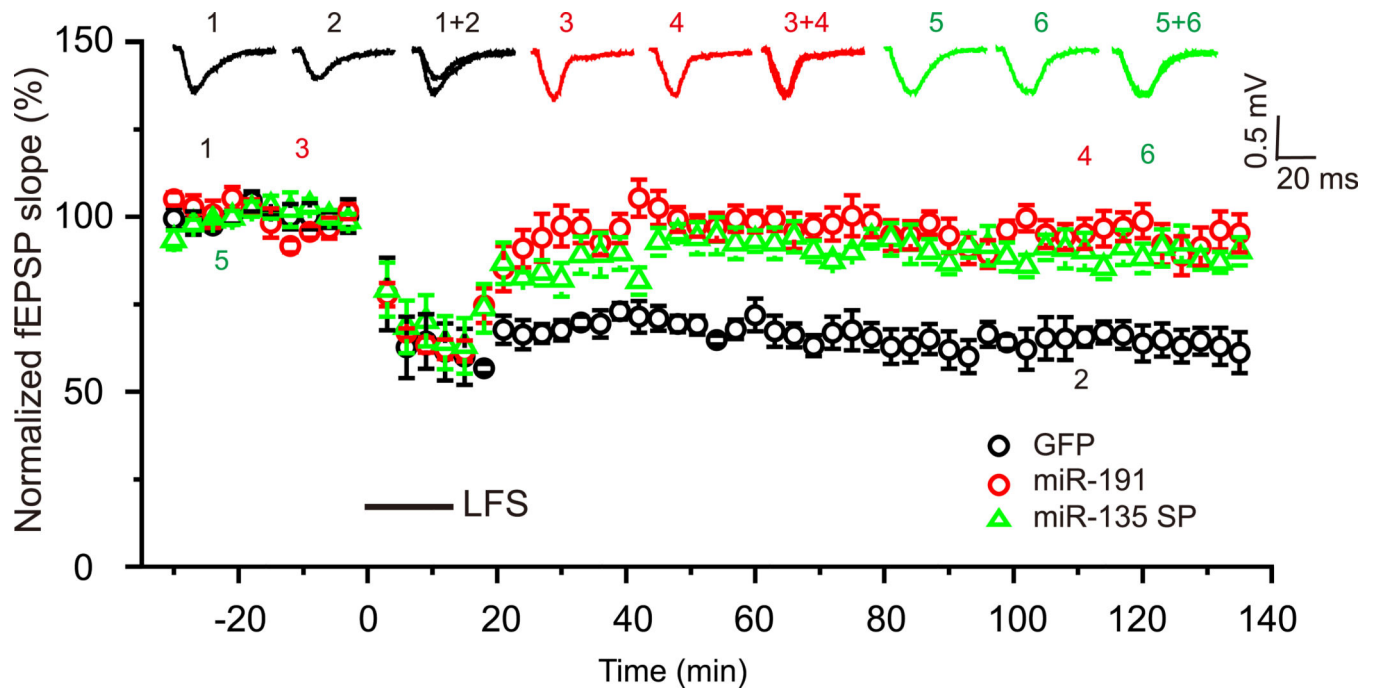
for each group. Data are presented as mean  $\pm$  SEM. Mann-Whitney U test was used for statistical analysis of the NMDA treated, DsRed and GluA1-SEP transfected group vs. other groups. \*  $p < 0.05$ , \*\*  $p < 0.01$ , \*\*\*  $p < 0.005$ . Scale bars, 10  $\mu\text{m}$ .

Author Manuscript

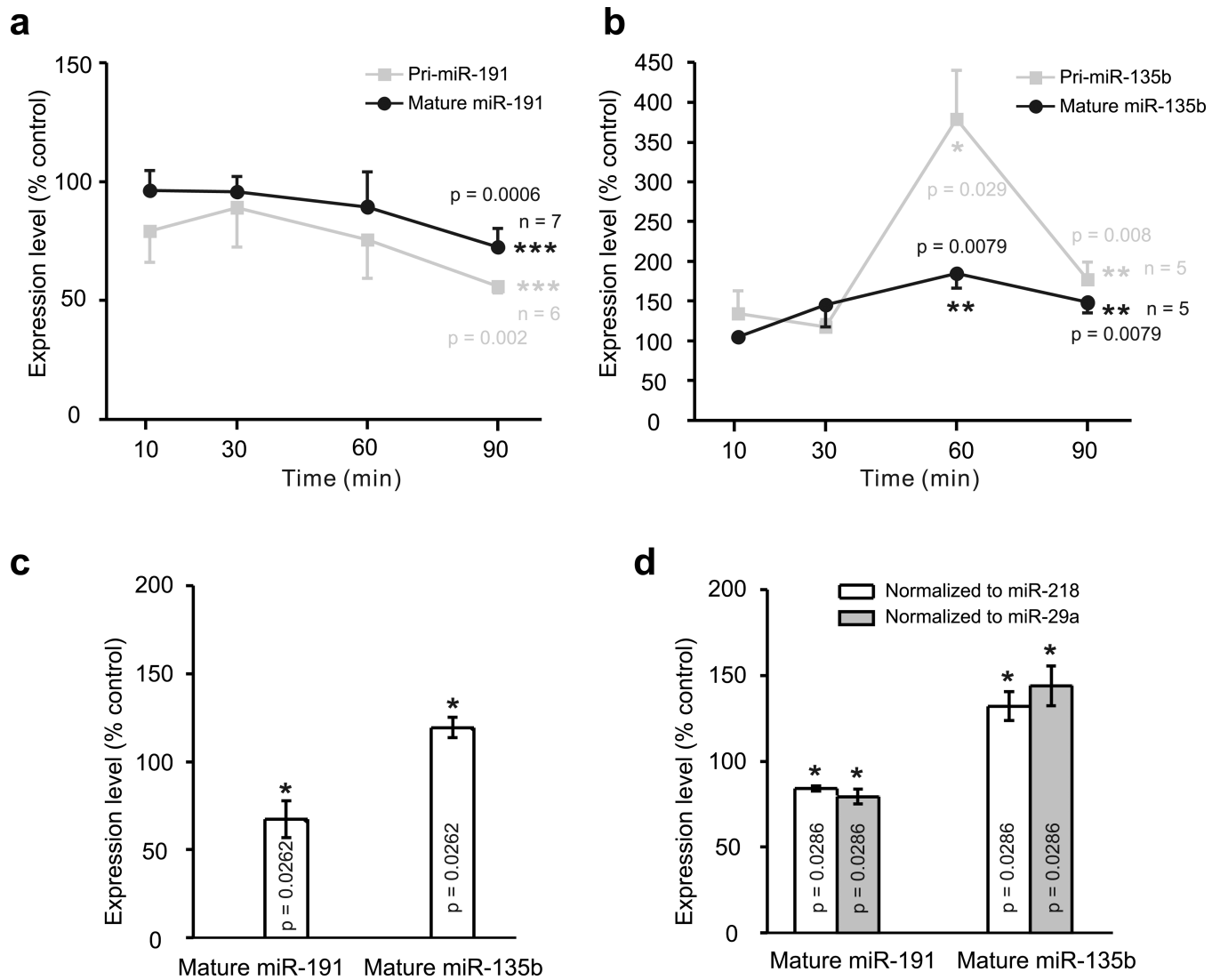
Author Manuscript

Author Manuscript

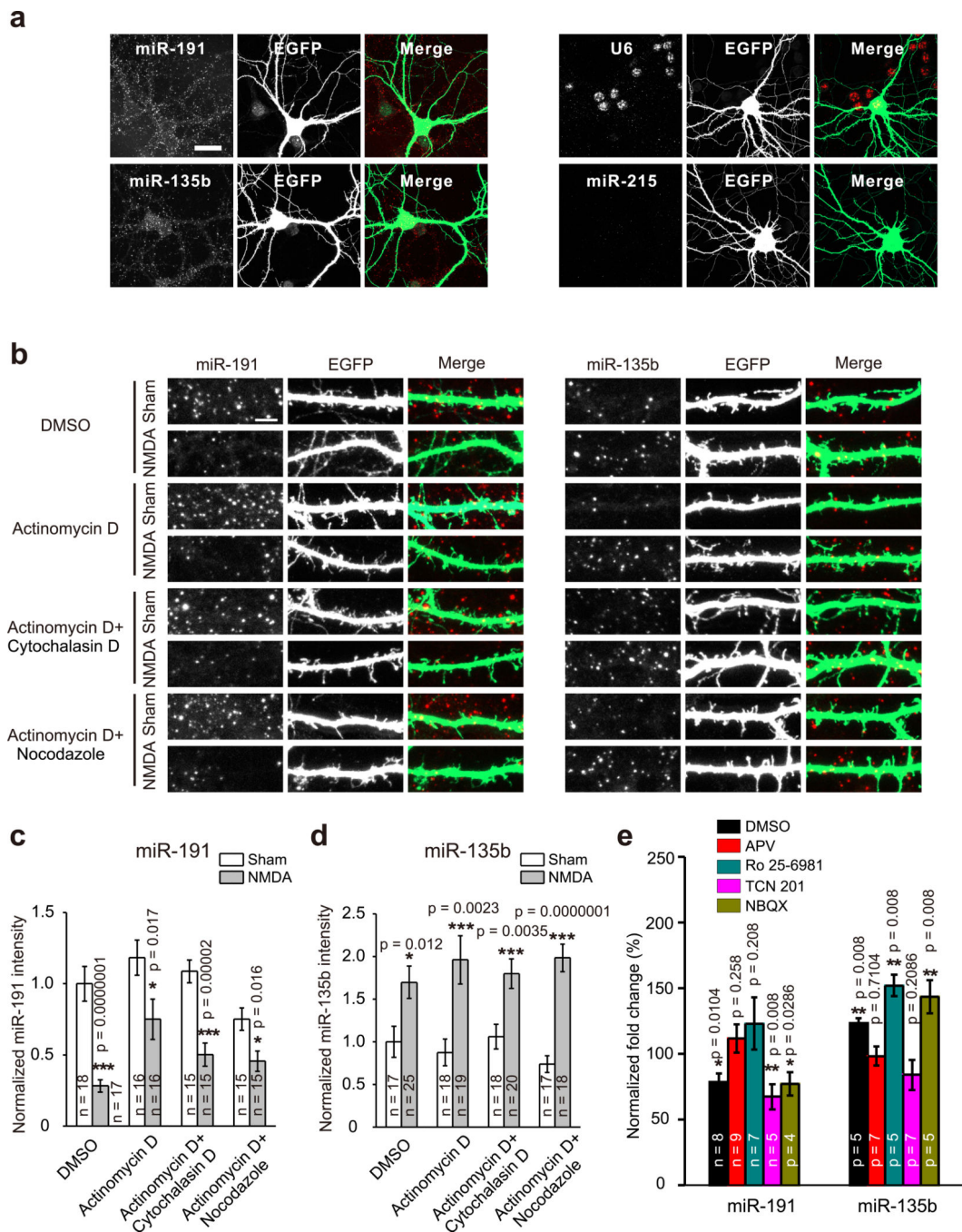
Author Manuscript



**Figure 8.** miR-191 and miR-135 are involved in LTD induction. Cultured hippocampal slices were transduced with lentivirus expressing miR-191 or miR-135 sponge. At 5 days after transduction, LTD was induced in CA1 neurons by low-frequency stimulation (900 pulses at 1 Hz). fEPSP slopes normalized to the pre-stimulation baseline were plotted as mean  $\pm$  SEM.  $n = 6$  slices for each group.



**Figure 9.** miR-191 and miR-135 are modulated at both transcriptional and post-transcriptional levels in LTD. Cultured hippocampal neurons were treated with NMDA (30  $\mu$ M, 5 min) alone (a, b) or along with actinomycin (c), and collected at indicated time points for qRT-PCR analysis (a-c). Cultured cortical neurons were treated with NMDA (30  $\mu$ M, 5 min) and used for CLIP assay at 90 min after treatment (d). (a) Time course of NMDA-induced changes in pri- and mature miR-191; n = 4–7 experiments for each time point. (b) Time course of NMDA-induced changes in pri- and mature miR-135b; n = 4–5 experiments for each time point. (c) The effect of actinomycin on NMDA-induced changes in mature miR-191 and miR-135b; n = 7 experiments for each condition. (d) The change in miR-191 and miR-135b associated with RISC; n = 4 experiments for each condition. Data are shown as mean  $\pm$  SEM. Mann-Whitney U test was used for statistical analysis. \*  $p < 0.05$ ; \*\*  $p < 0.01$ , \*\*\*  $p < 0.005$ .

**Figure 10.**

miR-191 and miR-135 are regulated locally in dendrites by different NMDAR subunits. Cultured hippocampal neurons were treated with NMDA (30  $\mu$ M, 5 min) alone or along with various inhibitors as indicated, and used for ISH (a-d) or qRT-PCR at 90 min after treatment (e). (a) Subcellular localization of miR-191 and miR-135b. (b) NMDA-induced changes in miR-191 and miR-135b in dendrites. (c, d) Quantification of b;  $n = 15$ – $25$  neurons for each condition. (e) Regulation of miR-191 and miR-135b by different NMDAR subunits;  $n = 4$ – $9$  experiments for each condition. Scale bars: 20  $\mu$ m for low-magnification (top), and 5  $\mu$ m for

high-magnification images (bottom). Data are shown as mean  $\pm$  SEM. Mann-Whitney U test was used for statistical analysis. \*  $p < 0.05$ , \*\*  $p < 0.01$ , \*\*\*  $p < 0.005$ .

Author Manuscript

Author Manuscript

Author Manuscript

Author Manuscript